CRANFIELD UNIVERSITY

SCHOOL OF APPLIED SCIENCE
MSc BY RESEARCH

Academic Year 2013 - 2014

MATTHEW DOWNIE

Measurement of soil respiration and its isotope signature using an automated closed-chamber system

Supervisor: Prof. G. Kirk, Dr. M. Pawlett
JUNE 2014

This thesis is submitted in partial fulfilment of the requirements for the degree of Master of Science by Research

ABSTRACT

A variety of methods is currently used for measuring soil and plant respiration and its isotope composition. Limitations found in the literature show a lack of a single set of specifications for these measurements. This report details a unique laboratory at Cranfield University (the Wolfson Field Laboratory - WFL) containing automated gas flux chambers attached to planted soil lysimeters and capable of providing near continuous measurements of gas fluxes and their isotope composition. The research in this thesis was concerned with the ability of the WFL to measure CO_2 gas fluxes from plants and soil and their isotope composition. A specification for closed chamber methods was developed, the validity of these specifications tested, and the ability of the WFL to meet these specifications determined. The methods developed include a means of assessing the effects of gas loss processes both on the measured CO_2 concentration and the measured isotopic signature within a defined volume. Measurements of plant and soil CO_2 efflux in the WFL lysimeters and its isotope composition were used to infer the isotope signature of plant and soil respiration using Keeling plots. The results showed the specifications developed were valid although further work is required to determine the ability of the WFL to meet the isotope measurement specifications.

Keywords: Specifications, diffusion modelling, Keeling plots, diurnal variation, CO_2 analysis

ACKNOWLEDGEMENTS

This research would not have been possible without the help, guidance and occasional annoyance on the part of many people. I would therefore like to acknowledge, and thank, the following people and organisations for their support and guidance throughout my research.

Firstly my supervisors; Guy, Mark (Pawlett) and Mark (Kibblewhite). Your advice and guidance was greatly appreciated, even if it didn't appear so at the time.

Secondly, all the organisations involved with the funding of this research including Sercon, the Douglas Bomford Trust and the EPSRC. I would like special mention to go to Sam Barker, whose expertise and advice with the instrumentation was invaluable.

I'd like to thank my family who, over the last few years, have had to put up with my moaning – although not much has changed since – and have provided support outside of the academic theatre.

My thanks also go to my friends at Mitchell Hall. As with my family, you provided a place to vent my frustrations and a source of entertainment.

Finally, to Margaret and Paul. You may have thought it was a small thing, but permitting me to stay was something which I will be forever grateful.

TABLE OF CONTENTS

LIST OF FIGURES

LIST OF TABLES

1 INTRODUCTION

1.1 Biogeochemistry of Soils

1.1.1 Importance of soils in global C cycle

The link between greenhouse gas (GHG) emissions and global warming is now well established. This has resulted in a focus on methods to reduce emissions, particularly for the sources and sinks of CO_2[1], CH4, and NO_x[2-7] on land. For this, there is a growing need to measure the fluxes of these gases and their link between their sources and sinks.

The global carbon (C) cycle includes the terrestrial C cycle, of which soils are an integral part. They contain approximately twice as much C as the atmosphere[8] and more than two-thirds of the total C in the terrestrial ecosystem[9]. They are also viewed currently as a sink for atmospheric C [10]. This is supported by a study which found the fraction of anthropogenic CO_2 absorbed by global soils to have increased between the 1980's and 1990's (with 0·2 (± 0·7) PgC y^{-1} and 1·4 (± 0·7) PgC y^{-1} respectively)[10]. However, research has shown that between 1978 and 2003 there was a net C loss in soils in England and Wales[8]. This shows that processes within the soils can result in some becoming sources of C. Obtaining greater understanding of these processes and their dynamics will provide greater knowledge of how soils are influenced by the global C cycle through the regulation of atmospheric CO_2 and climate change[11].

1.1.2 Soil C Turnover

Soil C losses are normally in equilibrium with inputs. These inputs mainly arise from plant litter and exudates from plant root turnover[12]. These inputs have great diversity in their chemical composition. Examples include labile exudates (such as sugars; amino acids; and organic acids) from roots, proteins, senescent material from tissue turnover, and polysaccharide mucilage[12]. These make up rhizodeposition which has been extensively researched[12]. Soil C losses usually arise from soil respiration (R_S)[9; 11] which consists of autotrophic (R_A) and heterotrophic respiration (R_H)[11]. R_A is the faster turnover of labile C through root respiration and has been suggested to include associated mycorrhizal fungi and

other micro-organisms in the rhizosphere[11; 13; 14]. R_H, on the other hand, is the slower turnover of recalcitrant C stocks from soil organic matter (SOM)[11]. The presence of plant roots can increase the rate of R_H, thereby allowing it to be a measure of priming effects (short term changes to the turnover rate of SOM usually caused by increased levels of organic C)[15] on R_S. By quantifying and understanding C loss as a result of R_H, models can be developed containing greater confidence levels linking climate change to determining whether a particular soil is likely to remain a C sink, or become a C source[9].

SOM is critical for soil structure maintenance and provides C substrates to support food webs which include nutrient cycling and pollutant degradation[12]. This is important as climate change can affect SOM turnover, and consequently GHG emissions[16]. It has been found that increased in temperature can decrease production of SOM by accelerating its microbial decomposition[8; 11; 16] while increases in precipitation can decrease SOM decomposition by increasing soil moisture levels, and so, retarding aerobic microbial activity[8; 11; 16].

Land use changes also have an effect on SOM turnover. For example, UK peat soils have been estimated to comprise 12 % of the rural land and 43 % of the 'British organic C stock'[17]. Drainage of these areas allows for greater aeration, so changing the environmental conditions to better suit aerobic microbial mineralisation. This results in greater SOM turnover and CO_2 emissions[17].

1.1.3 Soil C Turnover Measurement Methods

Soil C turnover is a dynamic process[16]. To understand the response of SOM turnover to environmental changes (changes in atmospheric CO_2, temperature, rainfall, land management), it is necessary to separate measurements of R_S into its components: R_A and R_H. A number of methods have been developed for this. One approach is to separate roots from the soil, for example with mesh or girdling trees, thereby removing R_A. However, this does result in artificial R_A-less systems. A less disruptive approach is based on differences in the isotope composition of plant and soil carbon[12], whether natural or artificially induced.

Changing plant type (C_3 vs. C_4) within a soil can result in isotopic differences between plant inputs and SOM turnover as much as c.15 ‰[12]. Typical C_3 plants have carbon isotope ranges between -20 to -35 ‰ $\delta^{13}C$[18] compared to typical C_4 plant ranges of -9 to -17 ‰[19]. Artificial labelling is usually done as a pulse over a limited period (hours or days) to minimise use of isotopes which may be costly. However this results in non-uniform labelling of the plants because rapidly, and slowly, turned over pools are labelled differently so pulse labelling does not provide an absolute separation of plant and soil fluxes[12]. A complete separation is provided by continuous labelling. But controlled field methods for this have yet to be developed.

The basis of isotope measurements is as follows:

The standard system for expressing isotope ratios uses the δ notation where

$$\delta^{13}\mathrm{C} = \left(\alpha - \alpha_{\mathrm{std}}\right)/\alpha_{\mathrm{std}} \times 1000 \qquad \textbf{1-1}$$

where α is the ratio of ^{13}C to total C in the material of interest and subscript std indicates a standard reference material, Vienna Pee Dee Belemnite in the case of ^{13}C.

If δ_A is the $\delta^{13}C$ of CO_2 from plant and litter C (normally approx. -27‰ in C_3 species), δ_B that of CO_2 from soil organic matter (SOM) C (typically -23 to -25‰, i.e. 2–4‰ more enriched in ^{13}C than plant C), and δ_S is the $\delta^{13}C$ of CO_2 emitted at the soil surface, which is a composite of δ_A and δ_B, then the fraction ε of SOM-C in the emitted CO_2 is given by

$$\varepsilon = \left(\delta_S - \delta_B\right)/\left(\delta_A - \delta_B\right) \qquad \textbf{1-2}$$

The end members δ_A and δ_B can, in principle, be measured separately. Therefore, with sufficiently precise measurements it should be possible to separate plant and SOM respiration using the natural $\delta^{13}C$ signatures of C_3 plants and soil[11; 12]. However this requires considerable analytical precision and isotopic partitioning may be confounded by minor variations in isotopic discrimination (e.g. during plant water stress). A much larger difference in $\delta^{13}C$ between the plant

and soil pools can be created by artificially labelling plants by growing them in an atmosphere with CO_2 depleted or supplemented in ^{13}C.

1.2 Measurement Methodologies

1.2.1 Chamber Methods

These methods involve a chamber of a known volume being placed over an area of soil, and changes in gas concentrations are measured with respect to time. These chambers are closed off from the external environment and samples of gas within these chambers are removed for analysis[20].

Closed Chamber Methods

This method involves the interior of the chamber being sealed off from the external environment whilst measurements are being taken. The only gases available for analysis will then only be those contained within the chamber. Measurements can be taken at regular intervals throughout the period of time the chamber is closed to determine changes in the gas composition, or concentration[20]. These methods can also be referred to as Non-Steady State (NSS) chambers[21]. There are two types of NSS chambers: Dynamic and Static chambers[22].

Dynamic chambers tend to minimise some sources of major uncertainty in measurements[22]. This is achieved by deliberately varying the CO_2 concentration over time to reach values above and below that of ambient concentrations[22]. The pressure within the chamber is also equilibrated with the external atmosphere quickly (approximately 15 s) at the start of any experiments, and by minimising the number of leaks, the uncertainty also decreased[22]. The size of the chamber is a major factor in the timescales over which measurements can be taken as, over time, the concentrations within the chamber reach a point where the diffusion gradient is decreased, resulting in a decrease in flux[23]. This means that, for small chambers, measurement periods can only last for a few minutes, compared to larger chambers[21].

Static chambers involve the use of syringes for the removal of gas samples for analysis[22]. This adds uncertainty to the measured concentrations of gas. It has

been found that underestimation of the total flux can be detected with CO_2 analysis[22], and can be particularly pronounced with longer timescales for measurements[5]

NSS chambers have one main source of uncertainty: leaks within the experimental setup. This can include leaks between the chamber and the analytical instrument, or between the chamber lid and walls[22]. Temperature changes within the chamber can also have an effect on the measured flux[20]. This can result in the production or consumption of the gas of interest to be accelerated. The effects of temperature changes can be minimised by applying insulating or reflective materials to the chamber walls and lid to maintain the internal temperatures of the chamber relative to the external atmosphere[20; 21]. Another source of uncertainty is that from mixing[5]. A non-consistent diffusion of gas throughout the chamber headspace will not provide a general overview of gas concentrations within the chamber[3; 24]. Addition of a small fan to the chamber lid will aid in the mixing whilst also not affecting the overall flux by alterations to the dynamic pressure within the chamber headspace[22].

Open Chamber Methods

These methods can be referred to as SS chamber methods. This method required the addition of a continuous flow of external air into the chamber[20]. Therefore a leak is deliberately added to this system to allow a near-steady concentration of gas within the chamber. Analysing incoming *versus* outgoing gas provides a concentration difference. This difference correlates to the gas flux from the soil[20-22; 24]. This allows for better mixing within the chamber headspace, as well as longer measurement timescales. However, pressure differentials and changes in the environmental conditions within the chamber can become problematic[21; 22; 25]. The consequence of this issues can result in an overestimation of the overall flux[5; 25].

Comparison of Chamber Methods

For the research in this thesis, measurement timescales are aimed to be short. For NSS chamber methods, this is ideal, whereas Steady state (SS) chamber methods are preferentially suited to longer timescales of measurement. Due to

the instrumentation being used, and the aim for near-continuous measurements throughout a 24 hour period, the use of syringes, as with SS chamber methods, is unfeasible. However, mixing and potential leaks does pose an issue with NSS chamber methods which needs to be addressed in order to ensure minimal uncertainty arising from measurements of gas flux, or fractionation of the isotope signatures of the fluxes.

1.2.2 Micrometeorological Methods

Gradient Methods

Gradient methods take measurements at a number of heights. These methods can be based on atmospheric turbulent mixing between (usually) two heights of a specific atmospheric entity or scalars (e.g. CO2, temperature, etc.)[20] as with Aerodynamic Gradient methods (AGM) or rely on measuring energy fluxes as with Bowen ratio Methods (BRM). AGM has traditionally been applied to determining temperature fluxes over forests as well as for measuring trace gas samples[20; 26]. However, there are a number of issues with this technique; firstly, it is limited to only being effective above plant canopies due to a lack of turbulent mixing[20], secondly, there are a number of empirical assumptions which must be made in order for the measurements to be valid and finally, the requirement for air stability[20].

Conversely, BRM provides a number of advantages over AGM including lower cost[26], can be used within plant canopies and does not rely heavily on turbulent mixing[20]. However, more assumptions are required for this method to be successful[26], despite there not being a need for stability factors[20], and low energy situations, such as at night-time can result in larger uncertainties in the measurements[20]. Due to its primary function in measuring energy fluxes, it is not able to measure trace gases compared to AGM[26].

Direct Methods

Direct methods take measurements at a single height. These methods include Eddy Covariance (EC) and Relaxed Eddy Accumulation (REA). EC measures the flux of a scalar at a point height across perpendicular, horizontal wind

streamlines[20; 26]. By far the best occasion to apply this technique is if the technique is to be applied over flat terrain (i.e. with no hills) with the underlying vegetation extending for some distance upwind of the instrument and that there are steady environmental conditions[26] and one of the main advantages of this method is that it does not affect gas emissions from the soil as can be found with chamber methods[22].

For REA, air is collected into one of two sample reservoirs according to up or down-draught air which is then measured[20; 26]. The analysis results in identification of air components and their respective concentrations. As the gases are collected over a period of time before analysis, the gas concentration differences are much more pronounced thereby allowing for more detailed laboratory analysis[20]. Additionally, because this method collects air sample, thus enhancing the concentrations of gases within them, it is well suited for analysis and/or detection of trace gases or pollutants. This is beneficial when compared to EC as REA does not rely on fast-response sensors meaning that for situations where such analysis is required; EC is rendered unsuitable for the task. In general, analyses for fluxes of CO2 and water tend to be performed using EC whereas REA is more commonly used for biogenic and other trace gas analysis[20].

Comparison of Micrometeorological Methods

Gradient methods use simpler instruments and obtain a clear measure of the flux of different scalars over a specific range of heights. However if there is low turbulent mixing, (such as over forests) or low energy gradients (in the cases of AGM and BRM respectively), then these methods do result in poorer quality results with greater uncertainties. Direct methods have comparatively sophisticated instruments for measurements and analysis. Despite this, they function over low turbulent mixing areas and do not rely heavily on empirical assumptions and calculations.

Both Gradient and Direct methods require the use of large extended distances upwind of similar, if not identical, vegetation to measure. Additionally, they both struggle to perform accurate measurements over ice or water, thereby making

them inefficient methods for GHG measurements over e.g. polar ice caps or seas[20].

Comparison of sampling Methods

The choice as to which method, Chamber or Micrometeorological, to use is dependent upon a number of factors; (1) what sample size is being used? (2) what type of terrain is being studied? And (3) are the local meteorological conditions highly variable?

For small regions (e.g. a few square metres), Chamber methods would advisable when compared to Micrometeorological methods which would require areas of at least whole fields, and *vice versa*. However, by using Chambers – regardless of closed or open – the gas emissions from soils will be affected. This issue is not found with Micrometeorological methods.

Micrometeorological methods are generally dependent on the local meteorological conditions, with the consequence that, should the local weather become too adverse (e.g. too much or too little wind), then measurements develop inherent systematic errors. This issue is generally not found with Chamber methods. Conversely, mixing of sample gases for Micrometeorological methods is not as problematic as it is for chamber methods due to the dependence on the local meteorological conditions.

1.3 Gas Concentration Measurement Methods

1.3.1 Gas Chromatographic (GC) Methods

The discussion of this method focused purely on GC, not on any additional components that can be added. With this method, a mixture of substances are separated out and measured according to retention time and concentration. In general, the mixture is passed through a column from an injection part through to a detector. Within the column is a stationary phase e.g. silica, which acts as a retardant for the mixture and an inert carrier gas ‘pushes’ the mixture through the column. The column is usually heated to a temperature suited to the separation needs and time constraints of the analysis – too low a temperature would result in an extremely slow process and may even result in some components of the

mixture not leaving the column, whereas too high a temperature may not result in any separation at all. Additionally, the flow rate of the carrier gas needs to be carefully adjusted to allow maximum separation in ideally a short time for the same reasons as given for temperature.

For the stationary phase, the example given was silica, which is highly hydrophilic – therefore the more hydrophobic the component (e.g. CH_4), the less retention will be observed which results in that component eluting from the column quicker than a more hydrophilic component (e.g. CO_2). For the analysis of CH_4, CO_2, and N_2O; Porous Polymer Beads are the more common stationary phase and require a column approximately 1-2 m in length with a diameter of 3.2-6.4 mm and a column temperature of 30-70 °C[20].

The main drawback with this analytical technique is that it only gives quantitative information. It is capable of separating a mixture into its components, thereby providing information about how many components where in the mixture and their relative concentrations. What it does not do, however, is provide qualitative data, i.e. what each component is when this instrument is used as a singular analytical instrument. For that, further additional components need adding to the GC. In many cases, this is a Mass Spectrometer which has the benefit of being able to identify each component in the mixture as it eluted from the column, however, other techniques exist such as flame ionisation detection which is used for CH_4 detection, electron capture detection which can be used to detect compounds with high electron affinity such as N_2O and CO_2[20], etc.

1.3.2 Infra-Red Gas Analysis

Infrared Gas Analysis (IRGA) relies on vibrational spectroscopy. This involves the absorption of IR radiation across a heterogeneous bond, e.g. C-H in CH_4, being detected and measured relative to the incident radiation intensity. Any absorption will result in a difference in the measured (transmitted) radiation compared to the incident radiation.

The absorption of IR at a specific wavelength can be determined by using the Beer-Lambert Law[20];

$$I = I_0 e^{-kcd} \quad \text{1-3}$$

Where I and I_0 are the transmitted and incident radiation intensities respectively, k is the molar extinction coefficient for the wavelength in question, c is the concentration of the absorbing gas and d is the path length.

Consequently, using the Beer-Lambert Law and the IR spectrum obtained from the instrument, one can obtain structural information regarding the gas in the sample as well as the concentration of the gas. These two components provide both qualitative and quantitative information about the sample.

One of the main benefits of IR spectroscopy is that absorption for a specific bond type tends to fall within a specific region. Therefore, if measurements show an absorption between 4184 and 4219 nm, then the molecule being identified has a C=O group compared to measured absorptions between 1948 and 1968 nm which corresponds to water molecules[7]. As a result, this technique can have selectivity with mixtures of known gases by focusing analysis on specific wavelengths and consequently, only analysing one gas with no interference from the other gases in the mixture.

Another benefit of IRGA is that, because absorptions are reliant on the bond strength which is itself reliant on the masses of the two atoms at each end of the bond; if one atom was changed for a different isotope, the result would be a different bond strength, therefore a different wavelength of IR in order to change the vibrational energy level, therefore a different absorption peak. Indeed, for CO_2, there are two different regions over which absorption can occur by changing between $^{12}CO_2$ (with absorptions between 2390 and 2370 cm^{-1}) and $^{13}CO_2$ (with absorptions between 2280 and 2260 cm^{-1})[7].

1.4 Isotope Measurement Methods

1.4.1 Isotope Ratio Mass Spectrometry (IRMS)

IRMS focuses mainly on lightweight isotopes of biologically important elements (H, C, N, O and S) [20]. This analysis is aimed at determining the relative abundances of one isotope relative to a standard reference material. Table 1

below shows the isotopes measured by IRMS and their respective international standards. It must be noted that a limitation of IRMS is the requirement for samples to comprise of specific gases to be used for analysis. In the case of H_2O and CH_4, these molecules readily undergo polymerisation when ionised. Therefore chemical conversion of these components in the analysed mixture is required. In the cases of the elements listed above, the lighter isotope is always the more abundant. Consequently, by measuring the relative abundance of the heavier isotope, it can be determined whether the sample of interest contains and enriched or depleted concentration of the heavier isotope[20]. This difference is referred to as δ notation with units ‰ (parts per thousand or per mille) [7; 20]. The δ values are calculated as shown in Equation 1-4 using $\delta^{13}C$ as an example.

$$\delta^{13}\mathrm{C} = \left(\frac{\frac{\mathrm{C\text{-}13}}{\mathrm{C\text{-}12}} Sample}{\frac{\mathrm{C\text{-}13}}{\mathrm{C\text{-}12}} Reference} \right) \times 1000 \qquad \textbf{1-4}$$

Table 1 Isotope ratios measured using IRMS including international standards

Isotopes measured	Fixed gas Required	International Standard
$^{2}H/^{1}H$ (D/H)	H_2	V-SMOW
$^{13}C/^{12}C$	CO_2	V-PDB
$^{15}N/^{14}N$	N_2	Atmospheric N_2
$^{18}O/^{16}O$	CO_2	V-SMOW
$^{34}S/^{32}S$	SO_2 or SF_6	

1.4.2 Laser Spectroscopic Methods

Numerous spectroscopic techniques have been considered as alternatives to IRMS. These include Photo-Acoustic Infra-Red Spectroscopy (PAIRS)[27], Long Path IR Spectroscopy (HAWK)[27], Tuneable Diode Lasers (TDL)[28], Diode-laser IR spectroscopy (MATI)[29] and Optical Spectroscopy[30]. Continuous Flow (CF)-IRMS possesses higher precision (≤ 0.1 ‰[29] compared to 0.2 ‰ for TDL[28]) however,

unlike CF-IRMS, TDL is capable of measuring CH_4 and H_2O without the need for chemical conversion[28].

Bias is also a problem with spectroscopic methods. PAIRS was found to consistently measure data that was negatively biased when compared with the same sample data from CF-IRMS[27]. Additionally, Optical Spectroscopic methods were found to drift by a greater amount than CF-IRMS over a period of 6 days[30]. Furthermore, the dependence on mixing ratios for $\delta^{13}C$ measurements means that it requires the use of equations to correct for this drift[30].

Local meteorological conditions can also have an effect on PAIRS and HAWK measurements. The level of underestimation for PAIRS was 33 % that of CF-IRMS when measuring $\delta^{15}N$ in N_2O but increased to 66 % under windy conditions[27]. HAWK however was found to produce the best results when temperatures were below 30 °C and wind speeds below 3-4 ms^{-1} [27]. This issue does not occur for CF-IRMS.

Conversely, the ability to make measurements of concentration as well as isotopic ratios is a clear advantage over CF-IRMS. Of the methods mentioned above, MATI[29], is capable of doing this. However, it is only limited to measuring $^{13}C/^{12}C$ ratios: a disadvantage when CF-IRMS is capable of measuring several isotopic ratios[29]. Speed is also an advantage of PAIRS[27; 29; 30], MATI and Optical Spectroscopy, thus allowing for real-time measurements[27; 30]. Furthermore, the lack of portability, labour requirements and cost can prove problematic to CF-IRMS[28; 30]. However, as mentioned before, CF-IRMS is capable of measuring several isotopic ratios whereas, in the case of TDL, each instrument can only measure a single isotopic ratio: thus requiring several instruments to measure the same number of ratios.

1.4.3 Comparison of Isotope Measurement Methods

Mass Spectroscopy is an important tool for analysis of molecular samples and, when combined with GC and cryo traps, trace gases can be measured both qualitatively and quantitatively. The comparisons between isotopes for a specific element can provide an insight as to natural processes within the environment.

With this understanding of isotope ratios from the environment, it can be determined as to whether specific environmental conditions result in a sink for heavier or lighter isotopes of e.g. carbon.

Much research has been performed to find other alternatives to CF-IRMS. The main benefits of CF-IRMS include the ability to measure several isotopic ratios within one single instrument, the associated (lower) cost of one instrument *versus* several instruments and higher precision. Consequently, at this point in time, CF-IRMS can still be considered a strong choice for isotopic analysis.

1.5 Introduction to the Wolfson Field Laboratory

The Wolfson Field Laboratory (WFL) was built for studying soil carbon dynamics and gas emissions. It is the focal point of the research detailed in this thesis and is the case study used for all experimentation described. The WFL contains 24 hydrologically-isolated soil monoliths (lysimeters; 12 each of two soil types) planted with grass and connected to automated gas flux chambers and instruments. The lysimeters are 0.8 m in diameter and 1 m deep, i.e., at least the size of a representative soil pedon, and therefore representative of field soil conditions. They are buried so that the soil surface is flush with the surroundings. Each is equipped with systems for controlling soil moisture and temperature, and instruments to allow near continuous sampling of gases emitted from the surface, dissolved solutes passing out of the bottom, and temperature and moisture at different depths. The layout of the WFL is shown in Figure 1. The gas flux chambers (26-cm head space) have pneumatically operated lids. Gases accumulated when the lids are closed are passed through a continuous sampling loop to an infrared gas analyser (IRGA) and an Isotope Ratio Mass Spectrometer (IRMS) housed in the instrument building. This allows simultaneous analysis of CO_2, CH_4, N_2O, N_2 and O_2 and their C, N and O isotope compositions. The IRMS software has been adapted to control the closing of the flux chambers and the directing of gas flow through the main sample loop to the chambers.

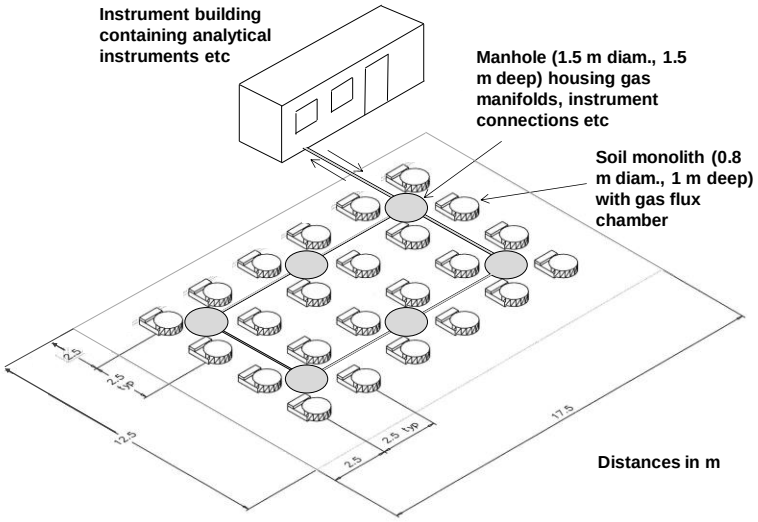

Figure 1 Layout of the Wolfson Field Lab

1.6 Flux and Isotope Measurement Specifications.

Among the issues found in the literature is that, for measurements of soil CO_2 efflux and its isotope composition, there isn't a single document which states the requisite specifications for such measurements to be valid. This is also important in developing new methodologies as there needs to be an ability to compare and contrast. The WFL was, until the research in this thesis, untested and the lack of specifications in the literature means that currently, there is no method of determining whether the measurements made are commensurate with those in the literature. To deal with this issue, the following specifications focusing on dynamic ranges, detection limits, sampling rates and acceptable errors.

1.6.1 Dynamic Ranges

Net soil efflux follows diurnal and seasonal changes with higher flux rates during night-times and in the summer, compared to daylight hours and in the winter[31]. The diurnal variation is as a result of photosynthetic activity. During daylight hours, the rate of photosynthesis is greater than that of soil respiration (R_S) whereas at night, photosynthesis is negligible such that the only changes in CO2 concentration over plant cover is through R_S[31; 32] and plant respiration (R_P). Seasonal changes arise from the seasonal variation in plant inputs to the soil and changes in soil temperatures and moisture levels. During the summer, when average temperatures and inputs of C to the soil from plants are greater, soil

activity is greater. Soil respiration is also affected by rainfall[31] and soil moisture content, tending to increase from dry to moist conditions but decreasing as the soil becomes anoxic due to excess moisture. Typical seasonal ranges in R_S in UK soils are from approximately 0.5 µmol $m^{-2}s^{-1}$ in the winter to approximately 4.5 µmol $m^{-2}s^{-1}$ in the summer[33]. The proportions of heterotrophic respiration (R_H) in R_S were found to vary across a dynamic range of 0.33 to 0.85[33]. These are the ranges the soil efflux measurements will need to cover in order for them to be within range of current models.

Table 2 Dynamic ranges of R_S, R_H and R_A

Respiration Type	Dynamic Range (µmol m^{-2} s^{-1})
R_S Total	0.5 – 4.5
$R_{H\ max}$[a]	0.425 – 3.825
$R_{H\ min}$[a]	0.165 – 1.485
$R_{A\ max}$[b]	0.335 – 3.015
$R_{A\ min}$[b]	0.075 – 0.675

a Values based on proportions of R_H in R_S

b Values estimated from difference between R_S and R_H

The ranges summarised in Table 2 are the ranges the soil efflux measurements will need to cover in order for them to be within range of current soil CO_2 efflux models.

The research being performed at the WFL uses a C_3 grass (meaning that the activation energies within the photosynthetic pathway preferentially use ^{12}C, compared to C_4 plants where the reaction cycles allow for more energetically efficient use of $^{13}C^{12}$) in soils where historical inputs were from C_3 plants. The history of C_3 inputs into soils results in the isotopic composition of older C stocks (the turnover of which dominates R_H) tending to be depleted in ^{13}C and its fractionation resulting in the measured isotopic composition of R_H falling within the range of -23 to -25 ‰, (i.e. 2–4 ‰ more enriched in ^{13}C than plant C)[11; 12]. C_4

inputs into soils, in comparison, tend to have the R_H fraction falling within the range of -9 to -17 ‰[19]. R_A, however typically has an isotopic signature of approximately -27 ‰[11; 12]. These typical $\delta^{13}C$ values provide the dynamic range for the isotope signatures from soil efflux. Atmospheric CO_2 typically has an average isotopic signature of approximately -7 ‰[32] . Therefore, the total dynamic range for the isotope measurements in the WFL system will be -7 to -27 ‰ (based on the two extremes of pure atmospheric CO_2 and pure R_A).

1.6.2 Detection Limits

The majority of models for soil efflux tend to work well under steady conditions, such as dry elevated CO_2 concentrations and ambient temperatures but tend to fail to fit the observed data when environmental changes are included (such as changes in soil moisture)[33]. Tests performed using different models have found that on average, the mean correlation coefficient (R^2) value between observed and modelled data was 0.7[33]. This suggests that 70 % of observed results within the dynamic range will be closely supported by modelled data. Therefore, the detection limit for the data must be 70 % of the dynamic range about the mean.

The precision of individual isotope measurements when using mass spectrometry is dependent on the concentration and volume of the introduced sample. The manual for the IRMS in the WFL states that the minimum concentration required needs to be similar to typical atmospheric concentration levels (approximately 350 ppm for CO_2) in order for analysis to provide reproducible measurements of the isotopic signature. IRMS systems are capable of working with samples with CO_2 concentrations equivalent to several thousand ppm[34]. It has been reported on several occasions that the samples sizes used for isotope was approximately 12 mL[11; 34-36]. Consequently, the detection limit for individual isotope measurements is based on the sample concentration and size which needs to be at least 350 ppm, and 12 mL respectively.

1.6.3 Sampling Rates

Sampling rates for soil efflux are dependent upon the method used. Flanagan *et al*[31] used eddy covariance in their research with flux measurements being made

over 30 minute sampling periods with mean data recorded every half-hour[31]. Throughout their work, 15 % of their data was rejected, or missing. The research being performed at the WFL uses a closed chamber system. Flux measurements for these systems are possible over a 10-15 minute time period[21]. The standard units for soil efflux measurements are μmol m^{-2} s^{-1}. The sampling rates found in the literature have are variable and some are described below:

Nagy *et al*[37]; took concentration measurements over three minutes and averaging concentrations over the last minute.

Davidson *et al*[38] took concentration measurements at 12 second intervals.

Livingston *et al*[23] performed similar experiments over 30 minute periods with measurements at five different points per experiment.

Langensiepen *et al*[39] performed measurements over 5 minutes at 1 s intervals, providing large quantities of data (300 data points) for efflux measurements per experiment.

Among the aims of the research at the WFL is the desire to take measurements on a near-continuous timeframe. To this end, soil CO_2 efflux measurements will be taken at 1 second intervals throughout the measurement period.

Typical isotope measurements using isotope ratio mass spectrometry (IRMS) use septum sealed vials and is capable of measuring typically 100 samples per batch[34]. The Continuous Flow (CF) system in the WFL allows for the use of sample vials to be avoided. Midwood *et al*[34] have found that CF-IRMS systems, like systems using septum sealed vials, are also able to measure approximately 100 samples per day.

1.6.4 Sources of Error

Closed chamber systems can result in underestimation of the total soil efflux[23] as a result of the diffusion gradient decreasing over time within the chamber due to the accumulation of efflux from the soil. Temperature changes within the chamber can also affect flux rates by accelerating the production or consumption of the targeted gas for analysis[22; 23]. Leaks within the system can also result in transfer

between the sample gas and external atmospheric air. To minimise uncertainties, the system needs to be leak-free with the chamber closed for a short enough period of time in order to obtain flux data, but not to eliminate the diffusion gradient between the soil and chamber headspace. Work by Livingston *et al*[23] has found that measurement error can be dependent upon the amount of sample handling. *In situ* flux measurements can have associated errors of < 0.1 % compared to extensive handling of samples providing errors between 1.5 and 2 %. Flux measurements will be performed in a similar manner to that by Langensiepen *et al*[39] which results in extensive sample handling. Consequently, flux errors should be no greater than 2 % to be comparable to the values determined by Livingston[23] and Langensiepen[39]. Comparisons between eight different models studied by Chen *et al*[33] have found that higher RMSE in modelled data resulted in a poorer correlation to the observed values. The best fit observed in the models examined had an RMSE of 0.24. An additional source of error will arise from diffusion within the Bev-A tubing used within the WFL[40]. The rate of diffusion of CO_2 through the tube walls must be accounted for in flux measurements[40]. The maximum error associated with the flux measurements for the research performed at the WFL must therefore be ≤ 2 % of the measured value (including the diffusion rate from the Bev-A line).

Isotope measurements are highly sensitive to fractionation. Leaks can therefore, not only affect concentration measurements, but can have a drastic effect on the measured isotopic signature as the sample becomes 'contaminated' with external atmospheric air. Fractionation, however, still occurs within soils with the soil CO_2 reservoir becoming ^{13}C enriched compared to the actual source by values up to 4.4 ‰. This is a result of kinetic isotope fractionation allowing $^{12}CO_2$ to diffuse more easily within the soil compared to $^{13}CO_2$. This is counter balanced at the soil surface resulting in this fractionation[34]. Other sources of uncertainty arise from the instrument itself. Adsorption and desorption effects can also introduce fractionation[41]. In the case of IRMS, this arises from ionised CO_2 adsorbing onto the flight tube of the mass spectrometer and later desorbing when being flushed in preparation for the next sample. This leaves active sites which preferentially adsorb CO_2 as more samples are measured; more active sites are created

ultimately generating a drift in the measured isotope signal. A solution to this issue has been suggested by Elsig *et al*[41] in which the use of a different compound (e.g. CO) with a stronger adsorption coefficient can be used to take up all potential adsorbing sites. The higher adsorption coefficient means that the conditions required for desorption are harder to meet. This will result in decreased fractionation within the mass spectrometer's flight tube and thereby minimising the effects of drift in the measured isotope signal[41]. The uncertainties with isotope signatures are typically given as ± 1SD which, because of advances within the mass spectrometric techniques involved are typically 0.1-0.2 ‰[34]. The maximum uncertainty within isotope measurements for this research will be set at 1SD = 0.1 ‰.

1.7 Aims and Objectives

The aim of this research is to determine whether the specifications outlined in 1.6 are suitable for the measurement of CO_2 flux rates and its isotopic composition for UK soils. The specifications will be applied to a case study (the WFL) using the following objectives:

1. To develop a series of test to determine the ability of the WFL to measure steady CO_2 concentrations
2. To measure CO_2 fluxes from the lysimeter chambers and to identify diurnal trends on these measurements
3. To develop the methodology to measure the isotopic composition of the CO_2 efflux during a sample run such that it is within the expected ranges.

2 GAS EQUILIBRATION AND LEAKS WITHIN SAMPLING LOOPS

2.1 Introduction

Understanding and quantifying sources of error in the WFL gas analysis system and the sample loops is important in determining whether the minimum specifications (1.6 can be met. To this end, the following experiments were made testing the different components of the WFL sample loops by measuring how well a steady CO_2 concentration can be maintained under closed-loop conditions. Potential sources of error include diffusion through the walls of plastic tubing (Bev-A line) or through poor seals at connection points, and isotope fractionation effects during the flow of the gas around the loops. The experiments were designed to systematically test the sample loop components, allowing each component to be assessed separately. Having identified any sources of error in this way, it was possible to systematically modify the system to minimise errors.

2.1.1 Gas sampling loops in the WFL

The main sampling loop in the WFL links the individual lysimeter gas flux chambers to the instruments in the instrument building via manifold substations (Figure 1 in Chapter 1). The loop comprises a main ring connecting the manifold substations to the instrument building, and secondary loops connecting the manifold substations to the individual flux chambers they serve. Two further sets of secondary loops connect the IRGA and the IRMS to the main loop in the instrument building.

The main sampling loop is made of 3/8 inch OD / 2/8 inch ID 316 stainless steel tubing. Its total length is 46 m but it is entirely gas impermeable. Potentially of greater significance in terms of gas leaks are the short secondary loops – which include some flexible plastic tubing – and their connections.

Figure 2 shows the secondary loop connecting the main loop to the IRGA. Air is pumped at approx. 1 L min^{-1} (the optimal rate for the IRGA) at 1 atm from the main stream through the IRGA using a diaphragm pump, needle valve and flow

meter. The pump is located downstream from the IRGA to reduce the effects of any pressure fluctuations it causes, which could introduce noise in the IRGA readings. The piping for the subsample loop is 1/4 inch OD / 1/8 inch ID PTFE tube. Measurements with a pressure transducer show that this arrangement produces pressure fluctuations < 0.01 atm at the IRGA. This is well within the IRGA's tolerance.

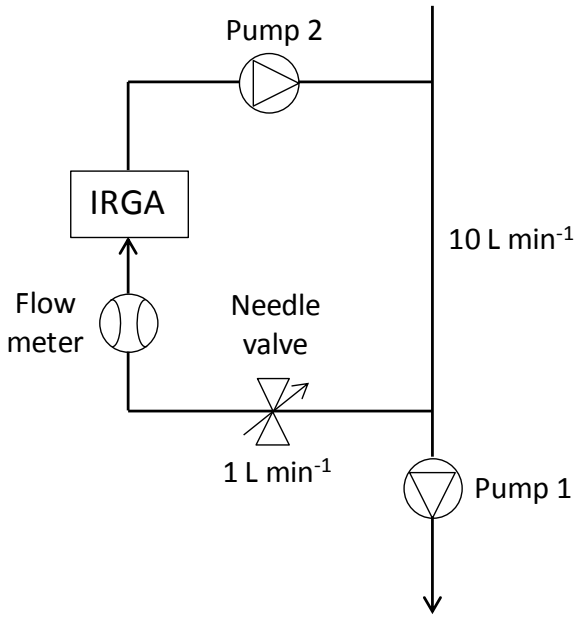

Figure 2 The sampling loop for the IRGA

Potential sources of error are leaks through the wall of the plastic tubing, and from the IRGA, flow meter, pump, and from the various connectors. This chapter is concerned with quantifying these potential errors and their significance in terms of the overall performance of the system

2.1.2 Aims and Objectives

Aims:

To quantify and minimise as far as possible sources of error in the WFL sample loops and to determine whether any residual sources of error are within acceptable limits as set in the generic specifications

Objectives:

a. To determine the effects of diffusion through tubing walls and poor seals on errors in concentration measurements.
b. To determine the effects of other components of the sample loop on errors in concentration measurements.

2.2 Materials and methods

2.2.1 Experiments

The most basic circuit (Circuit A, Figure 3) comprises an IRGA connected to a pump by tubing. The IRGA is a LiCor Li840A. The pump is a Charles Austen DA1 SE (1 L min^{-1} flow capacity). The tubing is 1/8" ID BEV-A line IV (supplied by Cole-Parmer Ltd) and it is connected to the IRGA and pump with push-on stud connectors (Camozzi 1510 Male Stud Taper 6/4).

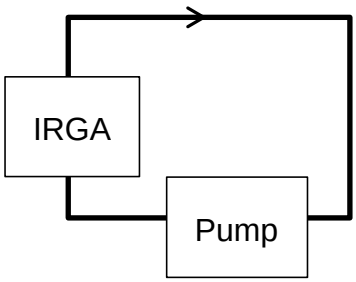

Figure 3 Circuit A

Circuit A was tested by introducing a pulse of CO_2 by blowing briefly into the tubing and then closing the circuit. The CO_2 concentration inside the tubing was then measured continuously (one measurement per second) for 5 min. This was repeated five times, equilibrating the air in the tubing with the lab air by pumping lab air through the open circuit for 5 min, before introducing each new pulse. The lab air CO_2 concentration was recorded before and after each pulse. This process was repeated using five lengths of tubing (297, 254, 208, 184 and 148 cm).

Additional sample loop components were then added to the loop in sequence (Figure 4), and the procedure for Circuit A was repeated. The additional components were:

1. a mixing jar containg a small electric fan to accelerate equilibration of the CO_2 pulse through the circuit (volume = 1000 cm^3);

2. a length of 1/8 inch ID stainless steel ‘pulse’ tube (introduced for other purposes, not discussed further; volume = 3 cm^3);
3. a portion of the 2/8 inch ID stainless-steel main sampling loop tubing, bypassing the main loop (volume = 1836 cm^3; NB losses will be similar for the total length of main loop tubing, being mainly through connectors, but equilibration is slower); and
4. the main sample loop pump (not switched on; volume of internal connecting space = 80 cm^3).

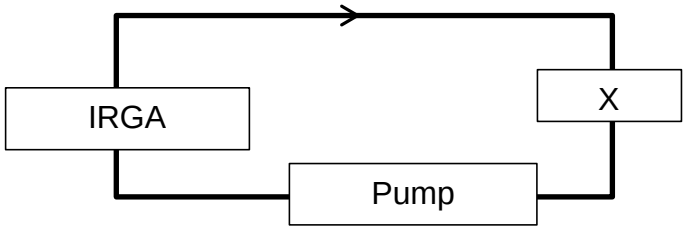

Figure 4 Modified Circuit A. Section X contains the additional component to be tested. In order of testing, these were (a) mixing jar, (b) pulse tube, (c) main sample loop pump (switched off) in series with mixing jar, and (d) the bypass loop in series with mixing jar

2.2.1 Analysis of results

2.2.2.1 Circuit A

In Circuit A, after the system has equilibrated following the addition of the CO_2 pulse, the rate of change in the amount of CO_2 in the tubing measured by the IRGA at a particular time is related to the rate of change in concentration by:

$$\frac{dM_t}{dt} = \pi a^2 l \times \frac{dC_a}{dt} \qquad \textbf{2-1}$$

where ;

M_t = amount of CO_2 inside the tubing at time t (mol)

C_a = Concentration of CO_2 inside the tubing at time, t (mol m^{-3})

a = internal radius of the tubing (m)

l = length of tubing (including that inside the IRGA and pump, as well as that outside which is varied) (m).

If losses are due to diffusion either through the tubing wall or through connectors, and in both cases are in proportion to the concentration difference between the inside and outside of the tubing (C_a-C_b, where C_b is the concentration outside in the lab air), then;

$$\frac{dM_t}{dt} = -\{\alpha(C_a - C_b) \times l + \beta(C_a - C_b)\} \quad \textbf{2-2}$$

where α and β are coefficients for diffusion through the tubing and from other loss processes respectively.

Combining Eqns 2-1 and 2-2 gives;

$$\pi a^2 l \times \frac{dC_a}{dt} = -\{\alpha(C_a - C_b) \times l + \beta(C_a - C_b)\} \quad \textbf{2-3}$$

i.e.

$$\frac{\frac{dC_a}{dt}}{(C_a - C_b)} = -\frac{\alpha}{\pi a^2} - \frac{\beta}{\pi a^2 l} \quad \textbf{2-4}$$

Therefore plots of $\frac{\frac{dC_a}{dt}}{(C_a - C_b)}$ against 1/*l* should have slope $-\frac{\beta}{\pi a^2}$ and intercept $-\frac{\alpha}{\pi a^2}$.

Values of dC_a/dt, C_a and C_b with which to calculate $\frac{\frac{dC_a}{dt}}{(C_a - C_b)}$ were obtained as follows.

Plots of measured C_a against time followed an exponential decline as C_a decreased towards C_b. Figure 5 gives an example.

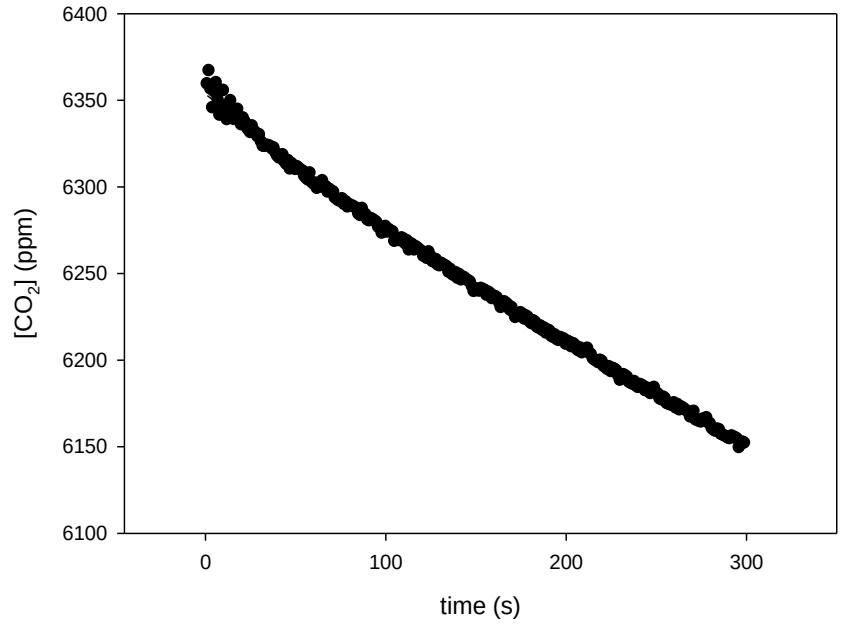

Figure 5 Example of change in CO_2 concentration inside the tubing (C_a) following addition of a pulse of CO_2 in Circuit A. The time t = 0 is set once the initial concentration has stabilised

These plots were well described ($r^2 > 0.9$) with the following equation:

$$C_a = C_{a0} + m \exp(-nt) \quad \textbf{2-5}$$

where C_{a0}, m, and n are constants. Differentiating Eqn 2-5 with respect to time gives

$$\frac{dC_a}{dt} = -mn \exp(-nt) \quad \textbf{2-6}$$

Eqn 2-6 can be used to evaluate dC_a/dt at any time t, and Eqn 2-5 can be used to find C_a at that time. For convenience, use $t = 0$.

Plots of measured C_b against time followed a slow linear increase as CO_2 accumulated in the lab (due to the presence of one or more respiring researchers). Figure 6 gives an example.

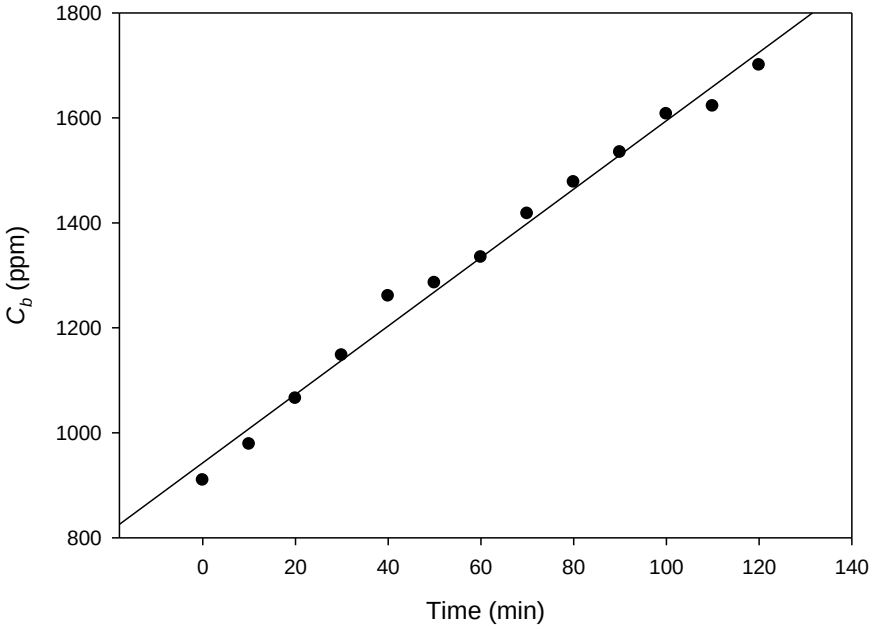

Figure 6 Changes in CO_2 concentration in the lab air outside the tubing (C_b)

Hence

$$C_b = C_{b0} + pt \qquad \textbf{2-7}$$

Where C_{b0} is the value at t = 0 and p is a constant. Therefore, for any particular run, the value of C_b at the time t at which dC_a/dt and C_a are evaluated can be found from Eqn 2-7 fitted to the C_b *versus* time data during the run, i.e. $p = (C_{b2}-C_{b1})/\Delta t$ where C_{b1} and C_{b2} are values of C_b before and after the run and Δt is the time interval between C_{b1} and C_{b2}.

2.2.2.2 Circuits with additional components

For additional components added to Circuit A, the equivalent forms of Eqns 2-1 and 2-2 are

$$\frac{dM_t}{dt} = V \times \frac{dC_a}{dt} \qquad \textbf{2-8}$$

and

$$\frac{dM_t}{dt} = -\{\alpha \times l + \beta + \gamma + \delta + \varepsilon + \cdots\}(C_a - C_b) \qquad \textbf{2-9}$$

where δ, γ and ε are coefficients for three additional components and V is the total volume of the revised circuit. The value of V depends on the components in the circuit. For example, for Circuit A combined with the mixing jar, $V = \pi a^2 l + V_{jar}$ where Vjar is the volume of the mixing jar.

Combining Eqns 2-8 and 2-9 and rearranging:

$$\frac{dC_a/dt}{(C_a - C_b)} = -\frac{\{\alpha \times l + \beta + \gamma + \delta + \varepsilon + \cdots\}}{V} \qquad \textbf{2-10}$$

To solve Eqn 2-10 for γ (and other components subsequently), the values of dC_a/dt, C_a and C_b are obtained as for Circuit A using Eqns 2-5, 2-6 and 2-7 fitted to the data for the new circuit. And substituted in Eqn 2-10 with the values of α and β found with Circuit A and the appropriate values of l and V.

2.3 Results and Discussion

2.3.1 Rates of loss from the circuits

Figure 7 gives typical examples of the time courses of CO_2 concentration inside the tubing following additions of a CO_2 pulse to the various circuits. An important section to consider is the plot for the bypass loop data as this test is the most similar to that for the main WFL sample loop. The fits of Eqn 2-5 to the data were made following the initial oscillation, and $t = 0$ set accordingly.

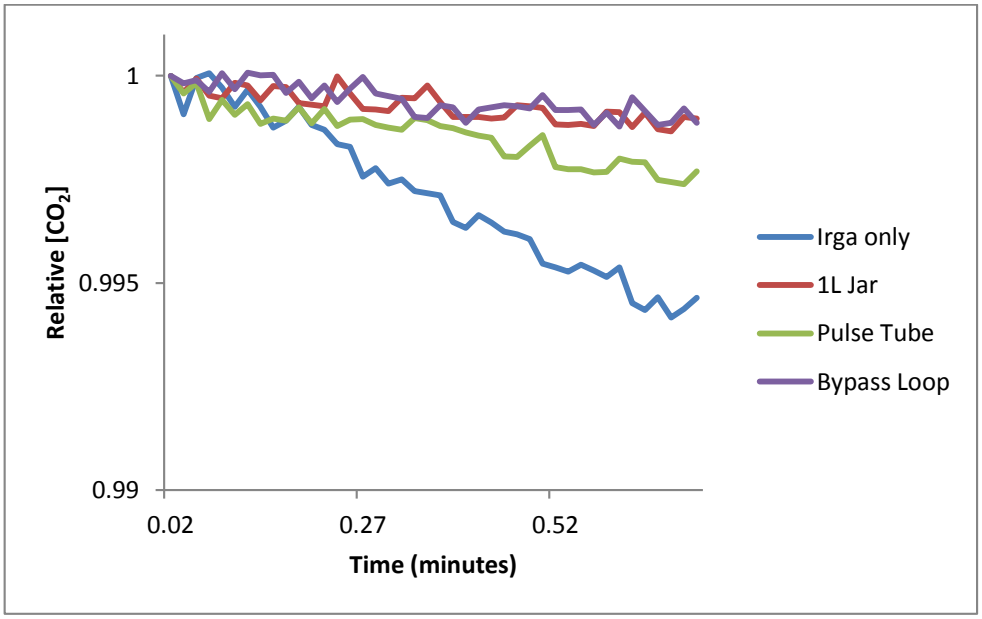

Figure 7 Example changes in CO2 concentration inside the tubing for the various circuits. The concentration is normalised with respect to the initial value in a particular run. Note the amount of CO2 in a given circuit is equal to the concentration multiplied by the circuit volume, and the circuit volumes differ greatly

2.3.2.1 Circuit A

Figure 8 shows the relative rate of concentration change ($\frac{dC_a/dt}{(C_a - C_b)}$) plotted against the reciprocal of the tubing length for runs with Circuit A. From Eqn 2.4 and the regression line fitted to the data, the values of α and β are 2.21 x 10^{-9} m^2 s^{-1} and 2.54 x 10^{-9} m^3 s^{-1}, respectively.

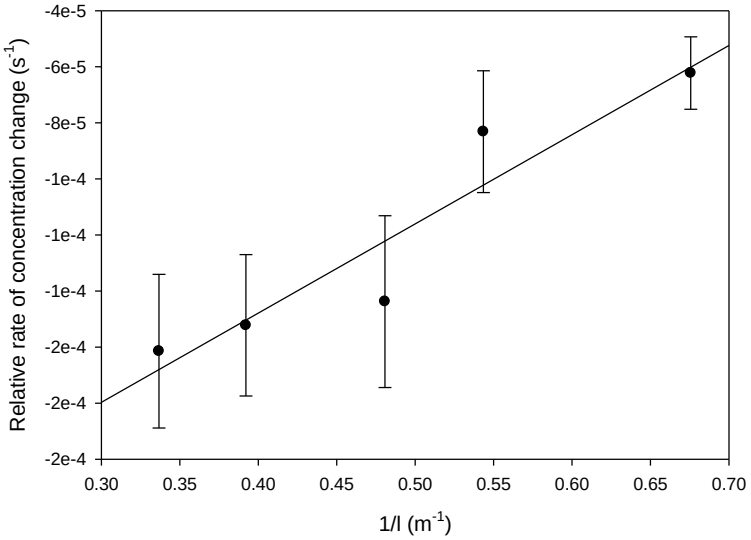

Figure 8 The relative rate of concentration ($\frac{dC_a}{dt}$) plotted against the reciprocal of the tubing length in Circuit A (cf Eqn 2.4). Data are means ± SD. The regression line fitted to the individual data has slope (= $-\frac{\beta}{\pi a^2}$) = 3.16 × 10-4 m s^{-1}, and y-intercept (=$\frac{\alpha}{\pi a^2}$) = -2.75 × 10-4 s^{-1}, r2 = 0.669, p < 0.0001

The value of α reflects the permeability of the tubing wall to CO_2. It can be used to calculate the apparent diffusion coefficient of CO_2 in the tubing wall – and so compared with published values for the materials the tubing is made from – as follows.

For steady-state diffusion through a hollow cylinder of internal radius *a* and external radius *b*, the quantity diffusing through unit length in unit time is (Crank, 1975[42], Eqn 2-11)

$$Q_t = -\frac{2\pi Dt(C_a - C_b)}{\ln(b/a)} \qquad \textbf{2-11}$$

Also, from Eqn 2-2,

$$Q_t = -\alpha(C_a - C_b)t \qquad \textbf{2-12}$$

Combining Eqns 2-11 and 2-12 and rearranging gives

$$D = \frac{\alpha \ln(b/a)}{2\pi} \qquad \textbf{2-13}$$

Substituting α = 2.21 × 10^{-9} m^2 s^{-1} and *b*/*a* = 2 gives *D* = 2.44 x 10^{-6} cm^2 s^{-1}.

The Bev A line tubing comprises a polyethylene liner with ethyl vinyl acetate shell. Gas diffusion coefficients in different polymers vary by several orders of magnitude, depending on the degree of sorption of the gas onto the polymer solid and diffusion through the solid matrix. Diffusion coefficients of CO_2 in polyethylene polymers at normal temperature and pressure (NTP – 298 K, 1 atm) are of the order of 10^{-6} cm^2 s^{-1} (Liao et al. 2013[43]; NB CO_2 diffusion coefficients are several times those for O_2). This is a little smaller than the value found above, but not far off.

A possible source of error in the above estimates is that the air inside the tubing may have been slightly over-pressurised by the act of blowing into it before closing the loop, resulting in subsequent pressure-induced mass-flow of CO_2 through the tube wall after the circuit was closed, in addition to diffusion. Without measurements of the pressure within the loop, it is not possible to account for this.

The reasonable agreement between the measured and theoretical diffusion coefficient indicates that the methods and analyses used here are sound.

2.3.2.2 Circuits with additional components

Table 3 summarises the coefficients for the tubing ($\alpha \times l$), other parts of Circuit A (β), mixing jar (γ), pulse tube (δ), the main sample loop pump (ε) and the bypass loop (ζ) obtained from this experiment. The values obtained for the bypass loop, main sample loop pump and the mixing jar were all greater than those from Circuit A, suggesting that is where effort to reduce losses, if needed, should be focused.

Table 3 Coefficients in Eqn 2-10 obtained for the various circuit components. The value of $\alpha \times l$ is for l = 2.08 m as in the amended Circuit A

Component	Coefficient	Value ($m^3 s^{-1}$)
BEV-A line tubing	$\alpha \times l$	4.60×10^{-9}
Other parts of Circuit A	β	2.54×10^{-9}
Mixing jar	γ	4.34×10^{-8}
Pulse tube	δ	1.10×10^{-7}
Main loop pump	ε	1.28×10^{-7}
Bypass loop	ζ	2.17×10^{-7}

2.3.2.3 Implications for the overall WFL sampling loop

Having calculated the coefficients in Table 3, they can be used to assess net losses from the overall WFL gas sampling system in relation to the much larger amounts of CO_2 contained in the main sampling loop and flux chamber head space.

The concentrations used to determine the coefficients were an order of magnitude greater than the typical concentrations expected in the lysimeter chambers during soil efflux measurements (these are in range 400–1200 ppm – Chapter 3).

Using Eqn 2-9, and normalising relative to C_a, we can determine the relative rate of loss of CO_2 as a function of C_a and C_b:

$$\frac{\Delta C_a/\Delta t}{\overline{C_a}} = k(\overline{C_a} - C_b) \qquad \textbf{2-14}$$

where k is the combined values of the coefficients, ΔC_a is the change in C_a over time interval Δt and $\overline{C_a}$ is the mean value over Δt.

Figure 9 gives plots of relative rates of loss using Eqn 2.14 assuming C_b is constant and equal to atmospheric CO_2 (i.e. C_b = 400 ppm), and using Δt = 600 s (i.e. 10 min, the typical time the lysimeter flux chambers are closed for flux measurements).

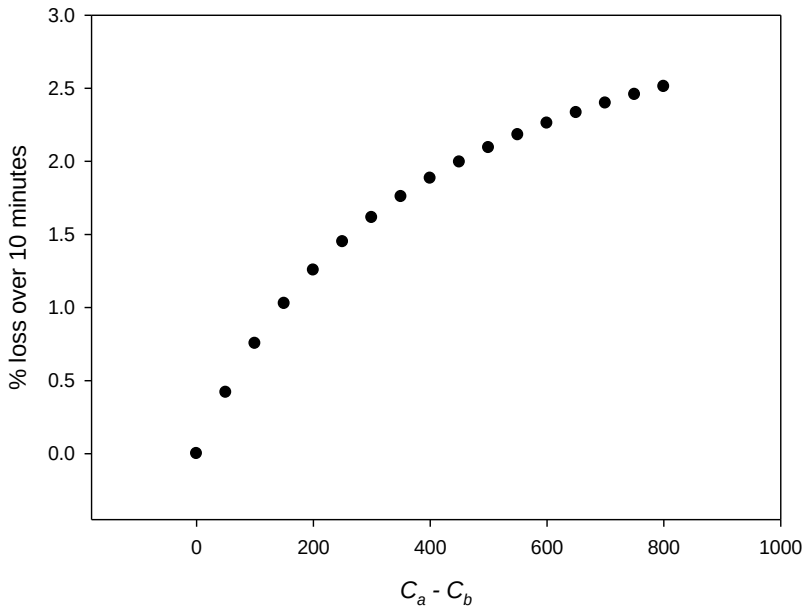

Figure 9 Percentage loss over 10 min as a function of the difference between internal and external CO2 concentrations, calculated with Eqn 2.14

From the plot in Figure 9, it can be seen that the percentage loss for a concentration difference of 800 ppm (i.e. C_a = 1200 ppm, which is the upper end of the range expected in the flux chambers), is 2.5 %, but the percentage losses are much smaller at smaller concentrations.

The total volume of the complete circuit including the mixing jar is 1.5 L. The volume of main sampling loop is 1.9 L, which is comparable. But the volume of the head space in the lysimeter flux chambers is much larger: 130 L. So the losses through the sampling loop components indicated here will be negligible in relation to the much larger quantity of CO_2 circulating through the chamber head space. Assuming similar loss rates through the full sampling system, the percentage losses of CO_2 in the whole the system will be in inverse proportion to the relative volumes, i.e. for the concentration range in Figure 7, the percentage

losses will be < 0.02 %. This is insignificant relative to the target accuracy of concentration measurements discussed in Chapter 1.

2.4 Conclusions

This series of tests were developed to assess how well a steady CO_2 concentration could be maintained in the WFL gas sampling system, and to assess the relative contributions of different components of the gas sampling system to possible losses of CO_2 from it. The results obtained showed connections between tubing and pumps etc were the most important sources of losses. But the overall losses were negligible in comparison with the amounts of CO_2 circulating through the WFL flux chambers under normal measurement conditions. The results were also used to determine the diffusion coefficient of CO_2 in the walls of the polymer tubing used in the sampling system. The diffusion coefficient obtained was slightly larger than published values for polymers; this may have been due to pressure-induced mass flow effects.

3 CHAMBER CO_2 FLUX MEASUREMENTS

3.1 Introduction

Flux measurements in an individual WFL lysimeter are made by closing the chamber lid, linking the chamber to an IRGA via the main sample loop, and following the change in CO_2 concentration in the chamber headspace over time. The CO_2 flux between the plant-soil system and atmosphere is interpolated from the rate of change in concentration.

There are a number of considerations to ensure any measurements obtained are useful. The lid needs to be closed for long enough to allow (a) the mixing of gas in the chamber and sampling loops to be complete, and (b) sufficient CO_2 accumulation in the chamber, after this mixing time is complete, to allow flux measurements to be made based on CO_2 concentration *versus* time plots. However the lid must not be closed so long that (a) environmental factors (such as temperature, humidity and pressure) within the chamber are changed, or (b) the accumulation of CO_2 in the chamber is so great that it affects the flux rate. In both cases, the result would be that plots of accumulation over time would become non-linear.

A further consideration is the effect of photosynthesis on CO_2 accumulation in a chamber. Through removing CO_2 from the chamber, the plotted accumulation over time would show either non-linearity, a decrease in CO_2 over time, or both. Measurements must therefore take into account the time they are taken, or the system needs to be designed to minimise the effects of photosynthesis. One method to minimise photosynthesis is to black out the chambers and has been performed on half of the chambers at the WFL.

3.1.1 Aims and objectives

The aim of the work in this chapter was twofold. Firstly, to quantify the differences in fluxes between seasons and diurnal patterns for individual soil types and individual chambers at the WFL. Secondly, to identify the limitations for

measuring fluxes and their effects. This was to be achieved through the following objectives;

1. To determine the optimum time intervals for the various stages involved in lysimeter flux measurements in the WFL system for different times of the year.
2. To quantify the differences in fluxes over diurnal patterns during different seasons
3. To quantify any similarities and differences between these measurements for individual chambers
4. To identify limitations from each of the above objectives and their subsequent effects on the measured fluxes.

3.2 Materials and Methods

The following sections detail the automation of the gas sampling from different lysimeter chambers in a particular experiment, the method for determining sampling time intervals, the determination of flux from CO_2 concentration measurements, and finally a summary of each of the experiments to be performed to fulfil the objectives above.

3.2.1 The Callisto Software

The entire sampling system is controlled by the Callisto software (Sercon v10.0.398) included with the IRMS. The valve and switch sequencing is defined using this software during any sampling process. There are six manifold substations, each linked to four lysimeters. The individual valves in a manifold substation can be activated in a specific sequence to connect an individual lysimeter 'in-line' with the main sample loop. The closing and opening of the chamber lids is also controlled by the software. All of these actions are also designated an individual time to occur thereby resulting in consistent, repeatable sampling sequences.

The software also determines the order in which individual lysimeters are sampled. It can randomise the order repeatedly (up to a maximum of seven times in one sampling process) such that two sampling batches (or lysimeter sampling

order permutations) are unique and different to each other. The result is that the time interval between repeat (three or more) samplings from the same individual lysimeter is not constant.

3.2.2 Flux measurement time intervals

During a set of measurements of gas fluxes, the chamber lids need to close and open in a random sequence and the relevant valves in the gas sampling loops opened. This is controlled by the Callisto software. During the interval between one lid closing and the next closing, there are four sub-intervals:

1. The time taken for the lid to close, Δt_1
2. The time taken for the air in the closed chamber and gas lined to equilibrate, Δt_2
3. The time taken for flux measurement, Δt_3
4. The time taken for the gas lines to re-equilibrate with the external atmosphere after the lid opens, Δt_4

Each of these intervals is controllable. The time interval between the start of the lid closing and the start of the lid opening ($\Delta t_1 + \Delta t_2 + \Delta t_3$) and the time from then to the start of the next lid closing (Δt_4) are specified in the relevant sequence table in Callisto. The time required for the lid to close (Δt_1) is altered by adjusting the pressure vent on the lid actuator (Appendix). The time allowed for the chamber air to equilibrate (Δt_2) -- i.e. the starting point used for interpolating the CO_2 flux from the measured data – is set such that the measured change in chamber CO_2 concentration has become steady, based on preliminary measurements. Then data from some part of the interval Δt_3, when the change in concentration over time is constant, is used to calculate the flux.

The following experiments were made to find appropriate values for these time intervals for reliable measurements of CO_2 fluxes in the WFL lysimeters. .

3.2.3 Determination of Flux

The CO_2 concentration (ppm, i.e. μmol CO_2 mol^{-1} air) is measured in individual chambers using the IRGA in the side loop off the main WFL sampling loop

(Chapter 2). The measurements are taken every second, and the rate of concentration change is obtained from the slope of plots of concentration against time.

The analysis will be based on the assumption that during the flux measurement period, the rate of plant and soil respiration is constant, resulting in a measured linear increase in CO_2 over time.

These plots will then be judged by eye to determine whether there is a linear increase in concentration and whether a linear regression is likely to provide valid statistics. The initial and final data point for flux determination will be identified from looking at all the original plots and chosen such that they avoid any non-linearity between the measured concentration and time. The data between these points will be used to determine a linear regression with an expected R^2 and p-value of >0.990 and < 0.001 respectively.

The equations detailed below demonstrate how the initial rate of concentration change (ppm s^{-1}) is converted into a flux (µmol m^{-2} s^{-1}).

The flux (*F*, µmol m^{-2} s^{-1}) is obtained from rate of concentration change (*dC/dt*) using the relation against time;

$$F = \frac{dC}{dt} \times \frac{N}{A} \qquad \textbf{3-1}$$

where *N* is the number of moles of air in the chamber, and *A* is the area of the chamber.

N is determined from the ideal gas equation;

$$PV = NRT \qquad \textbf{3-2}$$

where *P* is the pressure, *V* is the volume of the chamber, *R* is a constant and *T* is the temperature. As stated in section 3.1, the flux must be determined from the linear part of the concentration *versus* time plots.

3.2.4 Flux measurements

Throughout each of the experiments detailed below, the CO_2 concentration will be measured using a Li-COR 840A Infra-red gas analyser (IRGA) taking a measurement at a frequency of 1 Hz.

The first experiment will focus on determining Δt_1, Δt_2, Δt_3, and Δt_4. It will involve a single lysimeter where the lid will be deliberately closed for an extended period of time. This is to ensure that the point where the flux rate becomes affected is observed. This will be performed several times using multiple chambers at four points in the year (one per season). Each of the Δt periods stated above will be measured either through the timing of events, such as the opening or closing of the chamber lids, or from the collected data of CO_2 concentration *versus* time. These individual measurements will then be used for the following experiments in determining the flux.

The second experiment used eight lysimeters (four each of each soil type) which will be closed in a random sequence using the timings determined from the previous experiment. Each chamber was analysed for 15 minutes (covering Δt_1, Δt_2, Δt_3, and Δt_4). The chambers were closed for 9 minutes 40 seconds during each of these 15 minute analyses. The chambers will be measured repeatedly over 12 hour periods throughout the year. These measurements will be used to determine flux rate from each chamber using the equations from 3.2.3. From this, comparisons will be drawn between the flux rates of the two soil types and observations will be made regarding the seasonal variations of the flux.

The final experiment uses a single chamber throughout a 48 hour period, taking repeat flux measurements. The chamber itself was blacked out using (foil covered thermal insulation) to limit the effect of photosynthesis at any stage of the experiment such that only the effects of plant and soil respiration are measured. The measurements from this experiment will also provide further information regarding the diurnal pattern of the flux compared to the previous experiment.

From all of these experiments, the limitations of the system will be identified. These limitations will be used to identify likely occasions when flux measurements

would be adversely affected, resulting in more significant associated errors from the measurements.

3.3 Results and Discussion

3.3.1 Determining time intervals for flux measurements

Night-time measurements were performed to determine Δt_2, Δt_3, and Δt_4 in order to minimise errors arising as a result of ongoing plant photosynthesis during the day. These time intervals were determined through measuring the differing aspects of a chamber sampling process.

Each of the 24 chambers were individually closed then opened five times. The time period between the start and end of each stage, i.e. closing or opening, was measured using a stopwatch. The average time taken for any chamber lid to only close or open (Δt_1) took 20 seconds.

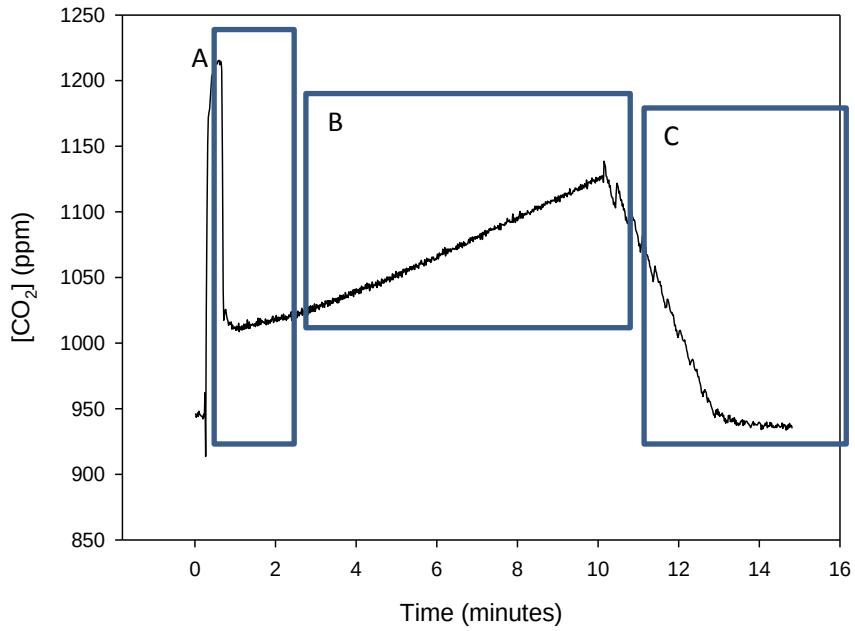

Figure 10 Example plot of chamber analysis for Δt_2 (A), Δt_3 (B), and Δt_4 (C)

Figure 10 shows a typical chamber analysis during a night time period. By measuring the time period between the points when the chamber is placed in-line with the sampling loop, the chamber lid closing, and a concentration change being detected, the value of Δt_2 can be determined. In the same way, measuring

the time period between the chamber lid opening and the CO_2 concentration returning to atmospheric levels, will provide Δt_4.

From this experiment, Δt_2 was calculated as 2 minutes from the point where the chamber was placed in-line, whereas Δt_4 was calculated as 5 minutes. Both of these time intervals included Δt_1 due to their being measured from the point when the manifold valves were placed in-line (in the case of Δt_2) and when the chamber lid was opened (in the case of Δt_4). When this experiment was performed in other seasons, the time interval for Δt_4 stayed relatively constant.

Therefore, irrespective of the time of year, the intervals for Δt_1, Δt_2 and Δt_4 can be considered as constants during any flux measurement period.

Determining Δt_3 is more complicated due to environmental factors affecting the flux rate. A concentration peak is achieved in a shorter time interval in the summer compared to in winter. In the subsequent discussions, Δt_3 is defined as the period over which the CO_2 *versus* time plot was linear in accordance with 3.2.3.

Considering the effect of seasonal variations throughout the year, the time period during which the lid is closed can be increased or decreased accordingly. The following table provides average Δt_3 values and flux rates for measurements taken during differing seasons.

Table 4 Average Δt_3 and Flux values determined at differing seasons

Season (year)	Δt_3 (n = 24)	Flux (µmol m^{-2} s^{-1}) (± 1 s.d.) (n = 24)
Summer (June 2012)	9 minutes	3.19 (0.5)
Spring (April 2013)	21 minutes 13 seconds	1.21 (0.6)
Autumn (October 2013)	9 minutes 40 seconds	1.49 (0.3)

The average flux values were based on the assumption that all the lysimeters were identical, irrespective of the soil composition within individual lysimeters and only the night-time measurements were considered.

The lack of winter measurements was due to unusual local weather patterns which made sampling difficult. This was as a result of heavy snowfall which acted as a 'barrier' to soil efflux, and heavy rainfall which waterlogged the site causing issues with other instruments including the soil probes for temperature and moisture measurements.

However, it can be estimated that Δt_3 can be up to three times greater in winter compared to the summer based on the similar difference between the spring and summer measurements seen in Table 4.

Among the limitations identified is that this research is based on measuring fluxes from UK soils under 'typical' UK weather conditions. As a result, extremes of weather, which cannot be usually predicted, will raise issues in identifying 'reasonable' fluxes on those occasions.

3.3.2 Multiple chamber measurements

Figure 11 shows an example plot of CO_2 *versus* time following a lid closing in eight chambers and their comparative flux rates during their measurement.

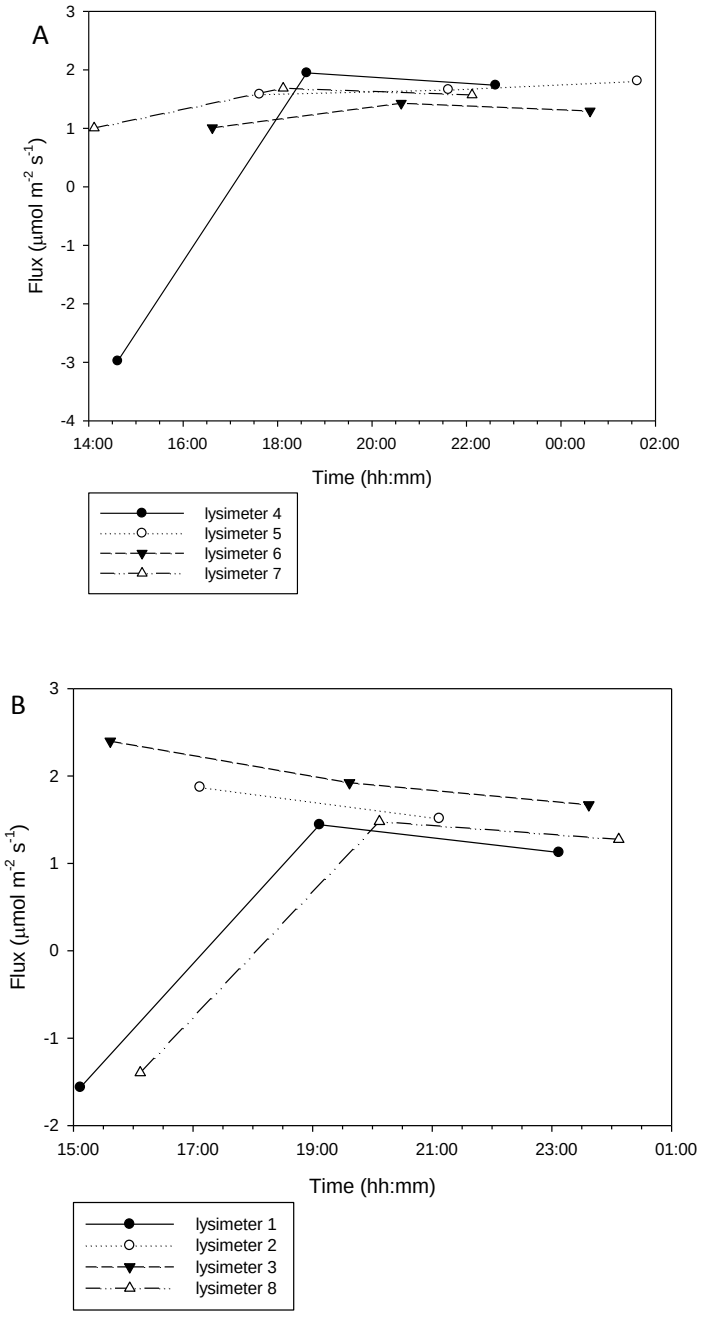

Figure 11 CO_2 gas flux measurements taken from multiple chambers over a 12 hour period. The night-time measurements (from 1800 hrs onwards) clearly show an accumulation of CO_2 while the day-time measurements show the effect photosynthesis has on CO_2 accumulation. A shows the fluxes form the Temple Balsall soils while B shows the fluxes from the Shuttleworth soils. In both plots, the filled circles and empty triangles were for non-blacked out chambers.

This pattern of change in CO_2 concentration for both the day and night-time measurements was replicated only in the non-blacked out chambers. The effectiveness of blacking out some of the chambers has been proved as a

consequence of obtaining 'correct' flux values during daylight hours (lysimeters 2, 3, 4, and 7).

Table 5 below shows the average flux rates for both soil types. From these averages, it is observed that there is some similarity between the fluxes measured from the same soil type.

Table 5 Average flux values determined from four lysimeters of each soil type. First average and second average refer to the second and third points for each of the flux measurements seen in Figure 11

Soil Type	Flux (1st average) (μmol m^{-2} s^{-1} (± 1 s.d.))	Flux (2nd average) (μmol m^{-2} s^{-1} (± 1 s.d.))
Temple Balsall	1.68 (0.21)	1.60 (0.23)
Shuttleworth	1.58 (0.22)	1.36 (0.23)

The standard deviations for the average fluxes determined from this experiment demonstrate that there is strong similarity between individual chambers containing the same soil type. However, there is a difference between the average fluxes of the two soil types. Subsequent tests, as summarised below in Table 6, aimed to determine whether these observed similarities and differences are statistically significant.

Table 6 Average CO_2 flux rated for two soil types in different seasons

Soil Type	Season	Average Flux (μmol m^{-2} s^{-1} (± 1 s.d.))
Temple Balsall	Summer (2012) (n = 18)	2.7 (0.5)
	Spring (2013) (n = 40)	0.9 (0.6)
	Autumn (2013) (n = 14)	1.5 (0.3)
Shuttleworth	Summer (2012) (n = 18)	2.5 (0.1)
	Autumn (2013) (n = 14)	1.6 (0.3)

An additional observation from Table 6 is that seasonal variations demonstrate further similarities between lysimeters of the same soil type. However, between the two soil types, the greatest variations in the measured fluxes are seen in the summer. The Measurements in the autumn, however, show much greater similarity between the two soil types. The lack of measurements in the spring was due to unusually high levels of rainfall which resulting in the Shuttleworth soils becoming waterlogged. This would affect any measurements of the flux and would not allow for direct comparisons between the free-draining Temple Balsall soil and the clay (non-free-draining) Shuttleworth soil.

The limitations identified from this work involve the ability to measure fluxes during the day. The chambers will need to be blacked out in order to take daytime measurements. This was performed in the next experiment.

3.3.3 Single closed chamber measurements

Figure 12 shows the flux variation over the first 24 hour measurement period of a blacked out lysimeter containing the soil from Temple Balsall.

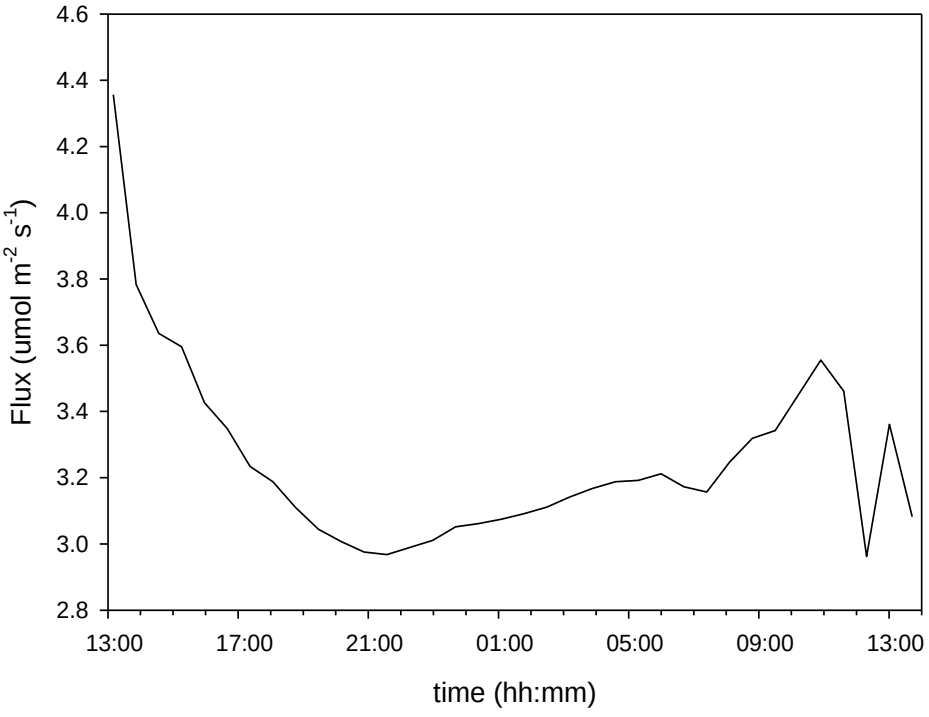

Figure 12 Plot of flux against time over a 24 hour period

From Figure 12 it is observed that, rather than the flux rate increasing at night compared to the day, the opposite is seen to be the case. An explanation for this is that the soil temperature at night is lower than during the day. Research performed on temperature dependence on soil respiration[44] has found two observations, the first of which applies to mid-latitude areas:

1. There is unlikely to be an optimum temperature for soil respiration under field conditions to be identified.
2. Both increases and decreases in soil temperature are matched by soil respiration.

From Figure 13, the soil moisture measurements appear to follow a similar trend to the observed fluxes in Figure 12. However, the soil temperatures do not follow this same trend.

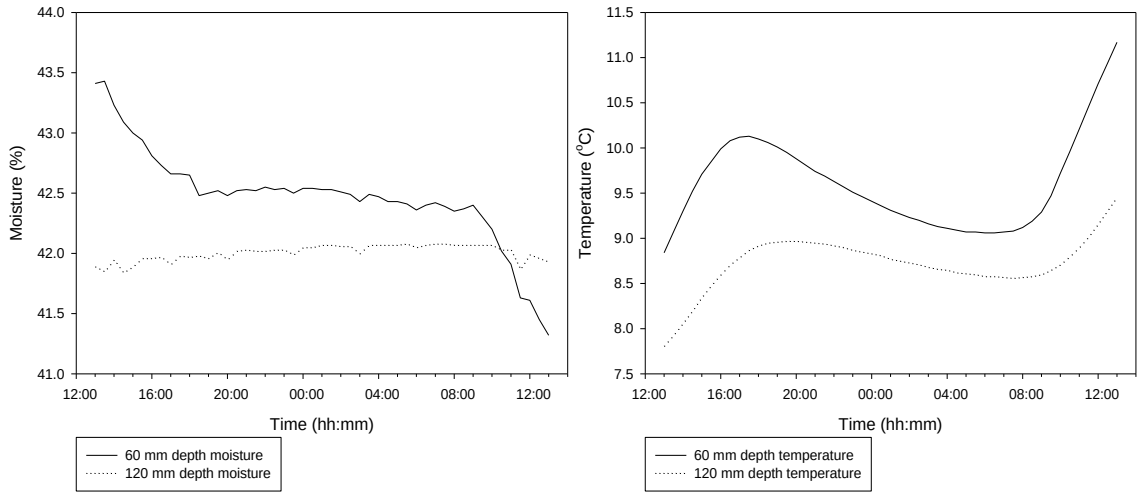

Figure 13 Soil and moisture data over a 24 hour period. NB; 60 mm and 120 mm refer to the depths at which these measurements were taken. The 24 hour period shown here is the same 24 hour period shown in Figure 12.

This observed link between the soil moisture and flux rate can be related to microbial processes within the soil. Increasing moisture levels would increase the ability of the microbial community within the soil to access soil carbon, resulting in increased waste production as measured through increased flux rates.

3.4 Conclusions

Experiments have been performed to determine the required time intervals for flux measurements, the variation of flux between differing chambers and differing times of the day, as well as the variation of flux over a 24 hour period for each, a closed and an open chamber.

The linear increase in CO_2 concentration has been identified from the first experiment to begin approximately two minutes after a chamber has closed and will continue for approximately ten minutes before non-linearity becomes an issue.

Issues observed for daytime measurements focus around photosynthesis. Non-blacked out closed chambers result in measurements demonstrating the plant photosynthetic rate as opposed to plant and soil respiration. This results in an apparent diurnal variation where the flux rate is greatest at night. However, from the closed blacked out chamber measurements, it was observed that flux rate is greater during the day due to increased soil temperature. Additionally, the same chamber, when kept open for the entire measurement period demonstrated more variation in flux measurements as a result of wind speeds. It also showed a similar trend to the closed blacked out chamber measurements in that there were higher flux rates during the day; however, the level of variation in the fluxes makes this observation difficult to uphold when considered without the closed blacked out chamber experiment.

To conclude, the WFL is able to measure soil efflux and is sensitive enough to demonstrate variations in a 24 hour period. Recommendations for future work would be to focus on the use of blacked out closed chambers to minimise the effects of photosynthesis and to perform the measurements of flux, soil moisture and soil temperature over multiple, consecutive 24 hour periods to observe the diurnal variation further.

4 MEASUREMENTS OF THE ISOTOPE COMPOSITION OF SOIL AND PLANT CO_2 EFFLUX

4.1 Introduction

A key feature of the Wolfson Field Lab (WFL) is its capacity to measure the isotopic composition of gases exchanged in plant and soil processes. The measured isotope composition can be used to attribute gas fluxes to their sources and sinks. This requires that the gases are sampled and analysed with adequate accuracy and precision and the aim of the work reported in this chapter was to assess this for measurements of CO_2 efflux from the WFL lysimeters.

During flux measurements, subsamples of the air circulating in the sample loop connecting individual lysimeters to the instrument building (see Fig .. in Chapter 1) are introduced into the IRMS and analysed for their CO_2 isotopic composition. The measured isotope composition over time in a closed dark chamber reflects the mixing of CO_2 in the air in the chamber when the lid is closed with the CO_2 produced in plant and soil respiration. The isotope composition of the respired CO_2 can be obtained from a plot of the measured isotope composition against the inverse of the CO_2 concentration[45] – so-called 'Keeling plots' – as follows:

If a fixed volume of air initially has concentration C_0 of a gas with isotopic composition I_0, and a source of the gas with a different isotopic composition I_1 is added producing concentration C_1, then, provided there are no other sources or sinks of the gas, as $C_1/C_0 \rightarrow \infty$, then $I_0 \rightarrow I_1$. The infinite ratio is approached when $C_1 >> C_0$. Hence, a plot of the isotopic composition of the mixture against $1/C$ (where $C = C_1+C_0$) will have y-intercept (i.e. $1/C = 0$) equal to the isotopic composition of the source of I_1.

Factors affecting the reliability of Keeling plots are as follows. A sufficiently wide range in measured C values is needed to allow extrapolation from the measured $1/C$ values to $1/C = 0$. However, as for flux measurements, the range must not be so large that the concentration increase over time is non-linear; any non-linearity indicates non-steady state diffusion of CO_2 from the soil, and associated

isotope fractionation (see Results and Discussion). Further, the isotope composition must be uniform throughout the gas sampling and analysis systems with no artificial fractionations. Finally, a sufficient quantity of measurements of concentration and isotope composition are required to produce statistically-meaningful Keeling plots.

4.1.1 Aims and objectives

The aim was to determine the ability of the WFL to measure isotope signatures of sufficient quantity and quality within a limited time interval to produce reliable Keeling plots, with which to infer the isotopic composition of CO_2 produced in plant and soil respiration. The following specific objectives were set:

1. To determine the minimum times required for individual isotope measurements during flux measurements.
2. To determine the stability of isotope measurements for a known source.
3. To produce Keeling plots from CO_2 efflux measurements in the WFL lysimeters.
4. To identify limitations in the WFL gas sampling and analysis systems and their effects on the Keeling plots produced.

4.2 Materials and Methods

4.2.1 The IRMS

A detailed explanation of the isotope sampling and analysis systems is provided in Appendix A. To summarise, an air sample of approximately 12 cm^3 volume is taken from the main WFL sampling loop via Valco valves, or a <1 cm^3 sample is taken from vials via an auto-sampler, then passed in a stream of helium into a 'cryo-loop' where CO_2 is concentrated by freezing. After thawing, the sample is passed onto a gas chromatography (GC) column where CO_2 is separated from other components, before being passed into the IRMS. At defined intervals, the cryo-loop is lowered into liquid nitrogen approximately 5 s before the introduction of the sample air from the Valco valves or auto-sampler. The valves are left open for approximately 30 s to allow full displacement of the sample air into the cryo-prep unit, before switching 'off' and placing in-line with the sample loop to refill

ready for the next sample. The cryo-loop is kept in the liquid nitrogen for a further 30 s before being raised to thaw. The sample is then passed through the GC column (Poropack QS) before being introduced to the IRMS unit.

The IRMS source is programmed to maximise the measurements of isotopes of mass to charge ratio (*m*/*z*) 44, 45 and 46. The area under each *m*/*z* line is used to determine the relative concentration of each isotope in the sample. Additional '2/1' and '3/1' ratios are calculated from the 45/44 and 46/45 *m*/*z* measurements, respectively. These are used to determine the isotopic composition of the sample.

The analysis involves the creation of 'integration windows' in the IRMS chromatogram. These have three components. The first is set over the period where the sample peak is expected to be detected. The other two are baseline regions set before and after the sample detection region against which the sample peak is integrated. The IRMS software then uses the information obtained from the integration to calculate the $\delta^{13}C$ of the sample.

After completion of the measurement, the next sample is introduced into the system. The overall sampling process is uniform regardless of the WFL chambers being analysed. This allows a consistent number of samples to be taken over the same intervals during a flux measurement.

The Callisto software of the IRMS system, used for the CO_2 flux measurements (Chapter 3), was also used to control the sampling and analysis of CO_2 isotope measurements.

4.2.2 Optimising the IRMS Settings

A series of experiments was performed to optimise the following sampling and analysis settings:

1. The sequence of reference and sample gas injections.
2. Sampling time intervals and the number of samples measured in a given period.
3. The time intervals for the IRMS chromatogram integration windows, ensuring entire sample peaks are captured.

The sequences and settings tested are given in the relevant sections of the Results and Discussion.

4.2.3 The Accuracy and Stability of Isotope Measurements

Three sets of experiments were made to test the accuracy and stability of the isotope measurements:

Firstly, by repeat injections of reference CO_2 gas directly into the IRMS, without passing through the cryo-loops or GC column. A total of seven repeat injections were used for each of the five tests performed.

Second, by repeat injections of air samples collected from the exterior of the lab in 12 cm^3 glass vials, and injected into the cryo-prep unit and IRMS via the auto-sampler. The vials (n = 10) were suspended above an individual chamber and left open to equilibrate with the external air for at least 4 hours. They were then capped with septa and analysed. Upon completion of the analysis, each of the vials was returned to the same location and the rubber seals were replaced. This process was repeated three times. The times samples were equilibrated with the external air was in the morning (approximately 1000 hrs on two consecutive days) and in the afternoon (approximately 1700 hrs on one day).

Third, by repeat injections of pulses of known CO_2 concentration circulated through a section of the main WFL sampling loop, bypassing the lysimeter flux chambers, and injected into the cryo-prep unit and IRMS via the Valco valve system. This used the truncated sample loop shown in Figure 4, Chapter 2. The total volume of air in the truncated sampling loop was 3 L, compared with 109 L in the whole sample loop plus flux chamber. Therefore, as for the CO_2 measurements in Chapter 2, any isotope fractionation due to losses from the system would have an amplified effect on the measured isotope composition. The CO_2 in the sample loop was removed using a scrubber (~50 g soda lime) to give a CO_2 concentration of ~0 ppm. A pulse of reference gas CO_2 was then introduced into the sample loop to provide sample loop concentrations of approximately 300 or 1200 ppm. The CO_2 concentration was recorded throughout and, once the concentration stabilised (i.e. there were no observable oscillations),

isotope measurements (n = 6) were taken. This was performed three times for each concentration.

4.2.4 Keeling Plot Measurements

Having optimised the IRMS settings for isotope measurements, measurements of the isotope composition of CO_2 efflux into lysimeter chambers were made, with which to construct Keeling plots. Four chambers of each soil type were used with flux measurements made consecutively over three days. Only the night-time measurements were used for Keeling plots; the daytime measurements are not discussed further. Three isotope measurements were taken per flux measurement period. This is the minimum number needed to produce a Keeling plot. The measurements were made at the height of the summer (July 2012) when plant and soil respiration rates were high.

4.3 Results and Discussion

4.3.1 IRMS set-up

4.3.1.1 Sample injection sequence

Figure 1 gives an example IRMS chromatogram for a sample injection sequence. The symbols are R = reference gas (against which all samples are compared), R' = reference gas used as a known sample, and S = actual unknown sample gas.

1. Injection sequence R, S, R', S, R'…

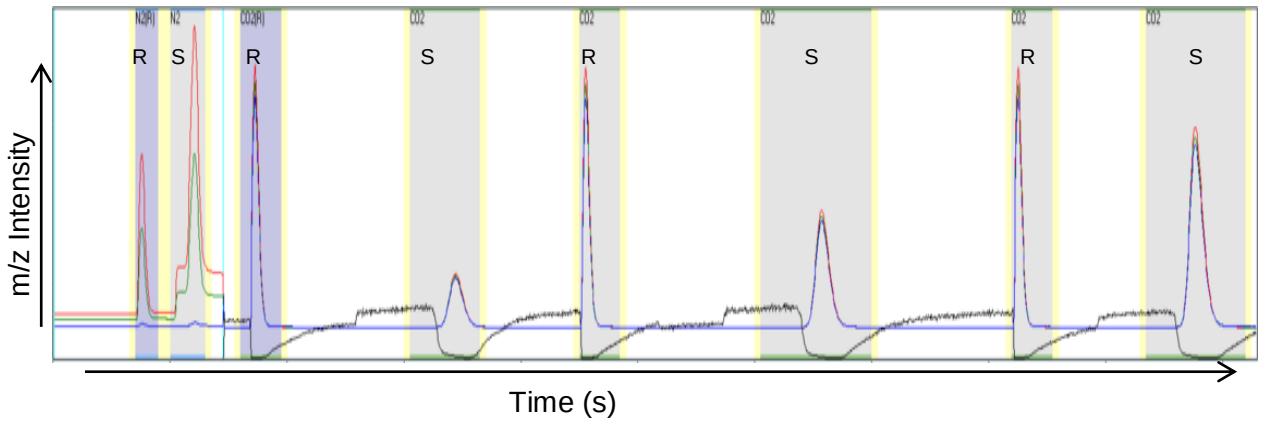

Figure 14 Illustrative chromatogram for the injection sequence R, S, R', S, R'… The coloured lines are for the different *m/z* values: red = 44, green = 45, blue = 46, black = 45/44 ratio. The first two peaks are for N_2; subsequent peaks are for CO_2. The shaded areas show

the integration windows: light yellow for baselines, light grey for samples. The darker shades are where the reference measurement is taken against which the samples are calculated. The labels above refer to N_2 or CO_2 and whether the peaks are from the reference gas (R) or sample (S).

In the sequence in Fig. 1 a reference gas was injected before each sample. The first of these was used as a reference, and each of the subsequent reference gas injections was considered as a sample. This was to determine whether there was any instrument drift over the period of measurement. The results in Fig. 1 are for three consecutive samplings from a closed, dark lysimeter chamber: the consecutive S peak areas and heights increase as CO_2 accumulates in the lysimeter chambers. Subsequent repeat measurements using the same sample gas gave $\delta^{13}C$ = -36.34 ± 0.3 ‰. This sample sequence was utilised for subsequent flux measurement periods.

2. Injection sequence R, R', S, S, …, S, S, R', R

This sequence involved a reference gas injection at the beginning and end of a sampling sequence. An additional reference gas injection was used as a sample either directly before or after the 'true' reference injection in order that any drift could be more accurately identified. This would allow for any instrumental drift in the sample measurements to be corrected for by the two identical reference injections. Six true samples were injected between the two end reference sample sets. Repeat measurements using the same sample gas gave $\delta^{13}C$ = -36.32 ± 0.2 ‰.

3. Injection sequence R', R, S, S, …, S, S, R', R

This final sequence involved a 'priming' reference injection followed by a 'true' reference injection. This allowed for any further purging of the instrument as a result of sample contamination within the detector before generating the reference measurement. Repeat measurements using the same sample gas gave $\delta^{13}C$ = -36.33 ± 0.3 ‰.

4.3.1.2 Comparisons between Sampling Methods.

4.3.1.2.1 Sampling Timescales

For all samples, the time from release from the cryo-trap to detection was 140-145 s. This interval could not be reduced without causing instrumental signal errors due to too high a carrier gas flow rate (originally set at approx. 10 ml min^{-1}). With the default instrument settings, the interval between sample introduction to the cryo-prep system and the cryo-loop being raised to thaw was on average 90 s. After some experimentation, the minimum period required for freezing and thawing, ensuring that the whole sample was introduced and collected on the cryo-loop, was found to be 60 s under the ambient, air-conditioned lab conditions. This results in a minimum total time for sampling and analysis, using the other default IRMS settings and the Poropack QS GC column, of 200 s. Thus, for a 10 min lysimeter flux measurement, a maximum of three samples can be taken for isotope analysis.

Further alterations to the analysis timings were performed to ensure whole peaks within the integration windows. For the example IRMS chromatogram shown in Figure 14, the total duration of the sampling sequence was 34 minutes.

4.3.1.2.2 Observations from the Sampling Process

After collecting the raw data, the software then applies a drift correction. From comparisons between the pre- and post-drift corrected results, minimal (< 0.01 ‰) drift was observed between the reference gas injections in any one measurement period. As the instrument is calibrated by the reference peak at the start of the measurement period, the results are expected to be accurate.

4.3.2 Accuracy and Stability of Isotope Measurements

4.3.2.1 Repeat Reference Gas Injections into the IRMS

This test involved the minimal components in the IRMS analysis system, i.e. the reference gas injected directly into the IRMS without passing through the cyro-loop or GC column. Repeat injections should show little or no drift. Each of the five tests performed followed the third method analysed in 4.3.1.1. Table 1 shows the standard deviation of the ‘samples’ and their average isotopic composition in each test. The aim was to have a standard deviation within the range 0.1-0.01 ‰.

Table 7 Average and standard deviations of the reference gas 'samples' from repeat injections (n=7 per test) into the IRMS.

Test	Average (‰)	Standard deviation (± ‰)
1	-36.30	0.03
2	-36.34	0.03
3	-36.33	0.04
4	-36.34	0.03
5	-36.26	0.05

From Table 7, the standard deviations fall within the range stated earlier. This therefore means that, by only using the minimal components, there is stability (i.e. no fractionation effects) within the measurements of the isotopic composition of CO_2 using the IRMS alone.

4.3.2.2 Repeat Measurements using the Autosampler

This expanded the number of components used by including the cryo-prep system and would determine whether any fractionation effects are observable as a result of the freeze-thaw process in the cryo loop sampling.

The use of ten vials could result in an issue where the identical composition of the contents of each vial is not assured. Realistically, the isotopic composition of the CO_2 in each individual vial would be unique. Thus, for the purposes of this test it was assumed that, after equilibration, the contents of all the vials were identical. Table 2 summarises the results from each test.

Table 8 Average Isotopic compositions of the vial air and their corresponding standard deviations

Test	Average composition (‰) (n = 10)	±1s.d ‰
1	-12.04	0.25
2	-13.28	0.96
3	-12.67	0.53

An observation from Table 8 is that there is variation between the average isotopic contents of the vials in each test. This can be explained as a result of the time of day they were measured. The first and third of these tests were performed at approximately the same time in the morning on two consecutive days. The second test, however, was performed in the afternoon of the first day when temperatures would have been higher and more plant activity would have occurred.

The observed variations in the standard deviations could also be explained in the same manner. As the tests were all performed at differing times, then other environmental factors, such as wind, temperature and rainfall (as occurred in the equilibration of the third test) would all have an effect on the isotopic composition of the air within the vials.

4.3.2.3 Known CO_2 Concentration Pulse Experiments

This final test involved the bypass loop and, compared to the previous tests, is the closest match to the 'real' experiment in 4.3.3.

The removal of CO_2 from the sample loop took approximately three minutes (see Figure 15). The scrubbing was continued for a further seven minutes before the pulse was introduced. From Figure 15 there is an observed oscillation in the measured CO_2 while the pulse becomes uniformly distributed across the sample loop. Approximately 15 min after the beginning of this experiment, the concentration has stabilised sufficiently for isotope measurements to occur.

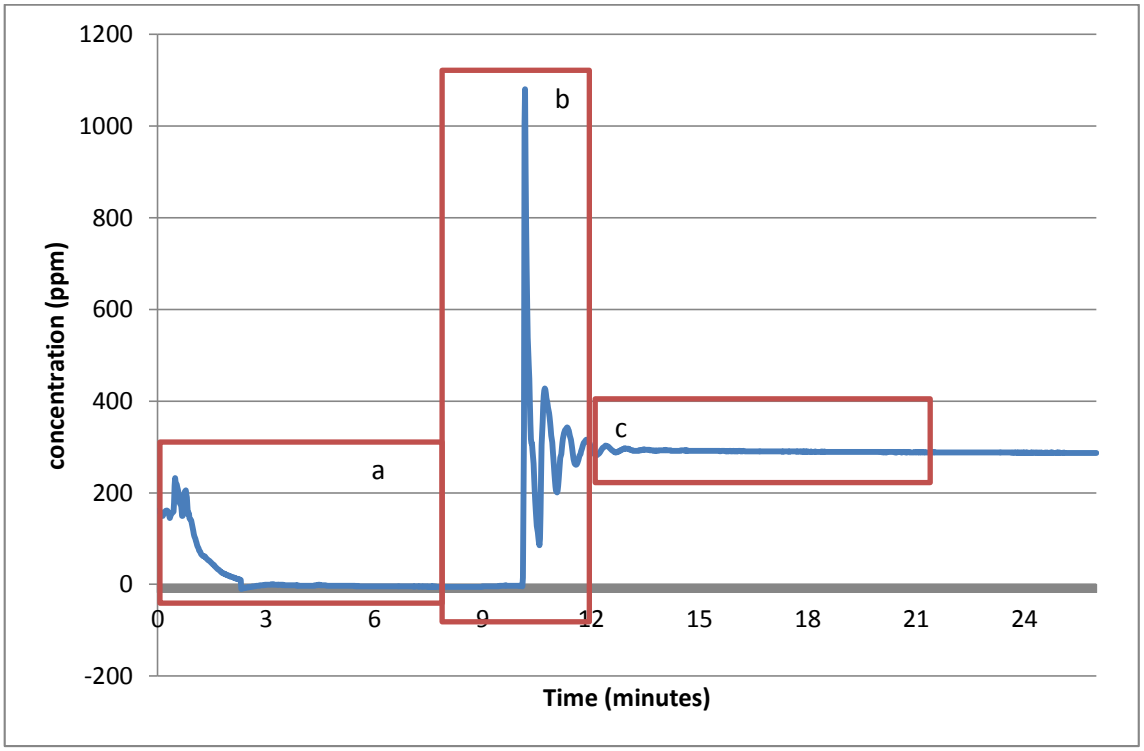

Figure 15 Mixing times for a 300 ppm CO2 pulse with a 1 L jar and LED fan included. a is the scrubbing period, b is the pulse mixing and stabilising period and c is the stable concentration period.

Table 9 below provides the average changes in isotope and concentration measurements during the pulse experiments. These were determined by calculating the difference between the first and last isotope measurement in each experiment and then taking their average. Potential sources of isotope fractionation include leaks in the tubing, particularly by diffusion through the walls of the Bev-A line tubing connecting parts of the system (Fig …, Chapter 2). The actual isotopic composition was not the focus of this experiment due to the fact that diffusion effects would occur throughout the pulse stabilisation period. As a result, despite the use of the reference gas for the pulses, the actual measured isotopic composition would be expected to be different.

Table 9 Average change in isotope and concentration of the introduced pulse (n=25 per concentration) over 42 minutes

Concentration (ppm)	Average $\Delta[CO_2]$ (ppm)	Average $\Delta\ \delta^{13}C$ (‰)
300	5.6	+1.11
1200	9.0	+0.34

Figure 16 below shows a typical plot of the changes in concentration and isotopic composition over time. Each of the points in the concentration plot were taken at the same time as the isotope measurement. The observed trend in decreasing CO_2 concentration and increasing $\delta^{13}C$ value over time was repeated in each test.

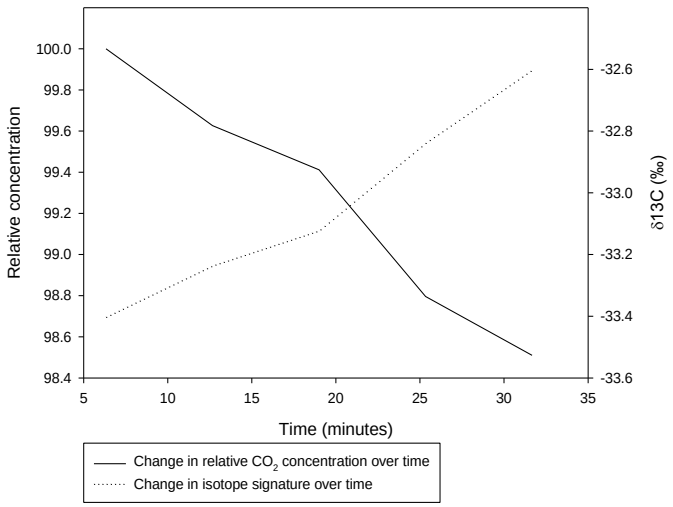

Figure 16 Typical plot of changes in concentration and isotope signature over time for the 1200 ppm pulse tests. The concentration values have been normalised relative to 1200 ppm. The base isotopic signature of the introduced pulse was -36.3 ‰. Diffusion and other fractionation effects resulted in the measured isotope signature being more positive.

From Table 9 the overall changes in the isotope measurements are small with changes of 0.37 and 0.03 % for the 300 and 1200 ppm pulses respectively. Due to the percentage of the loop comprising the plastic Bev-A line tubing in this experiment being much greater than compared to the main loop (3.3% compared to 0.09%), then the effect of diffusion is likely to be reduced when using the whole loop.

One of the limitations identified from this work is that the time taken to measure six samples from the loop was 42 minutes. From Chapter 3, this timescale is too great for the fluxes being measured. However, this is to be expected as the focus was to determine the stability of the isotopic signal over an extended period which was at least as long as a flux measurement period. The measurements, having been taken at seven minute intervals and an overall isotopic change of < 1 % from a combination of sampling and diffusion effects demonstrates that errors in

measuring the isotopic composition of the sample loop air will arise from the measuring of the flux.

4.3.3 Keeling Plot Measurements

Figure 17 gives plots of CO_2 concentration and Isotope signature *versus* time for 12 night-time measurements and Fig. 6 gives the corresponding Keeling plots.

(A)

Lysimeter 2 (040712)

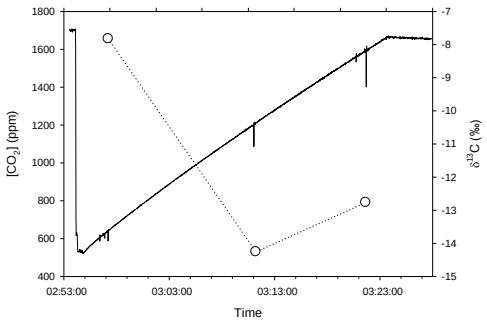

Lysimeter 2 030712

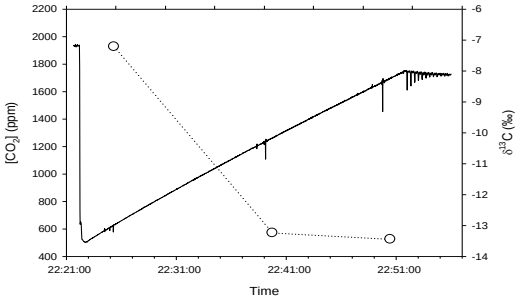

Lysimeter 2 (020712)

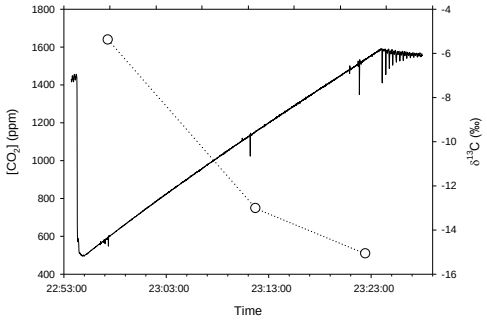

Lysimeter 3 (040712)

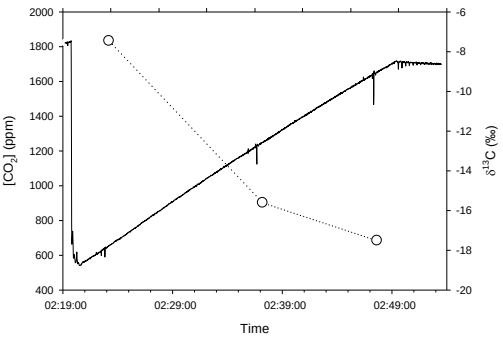

Lysimeter 3 (030712)

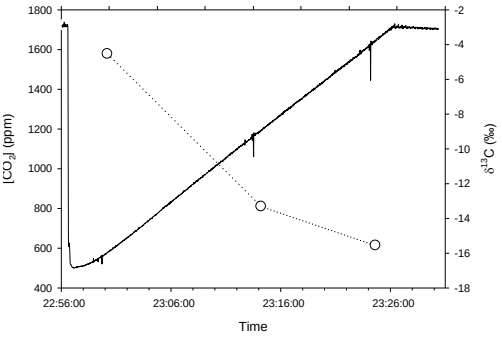

Lysimeter 8 (020712)

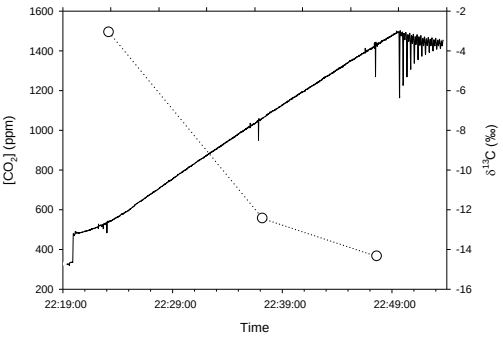

Lysimeter 10 (040712)

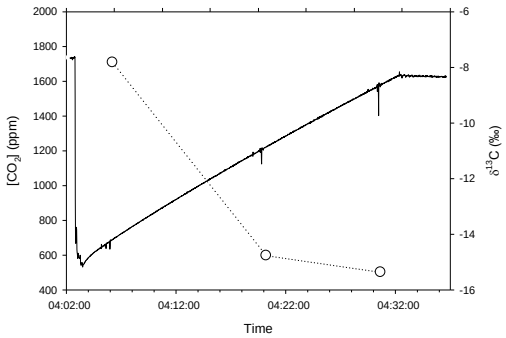

(B)

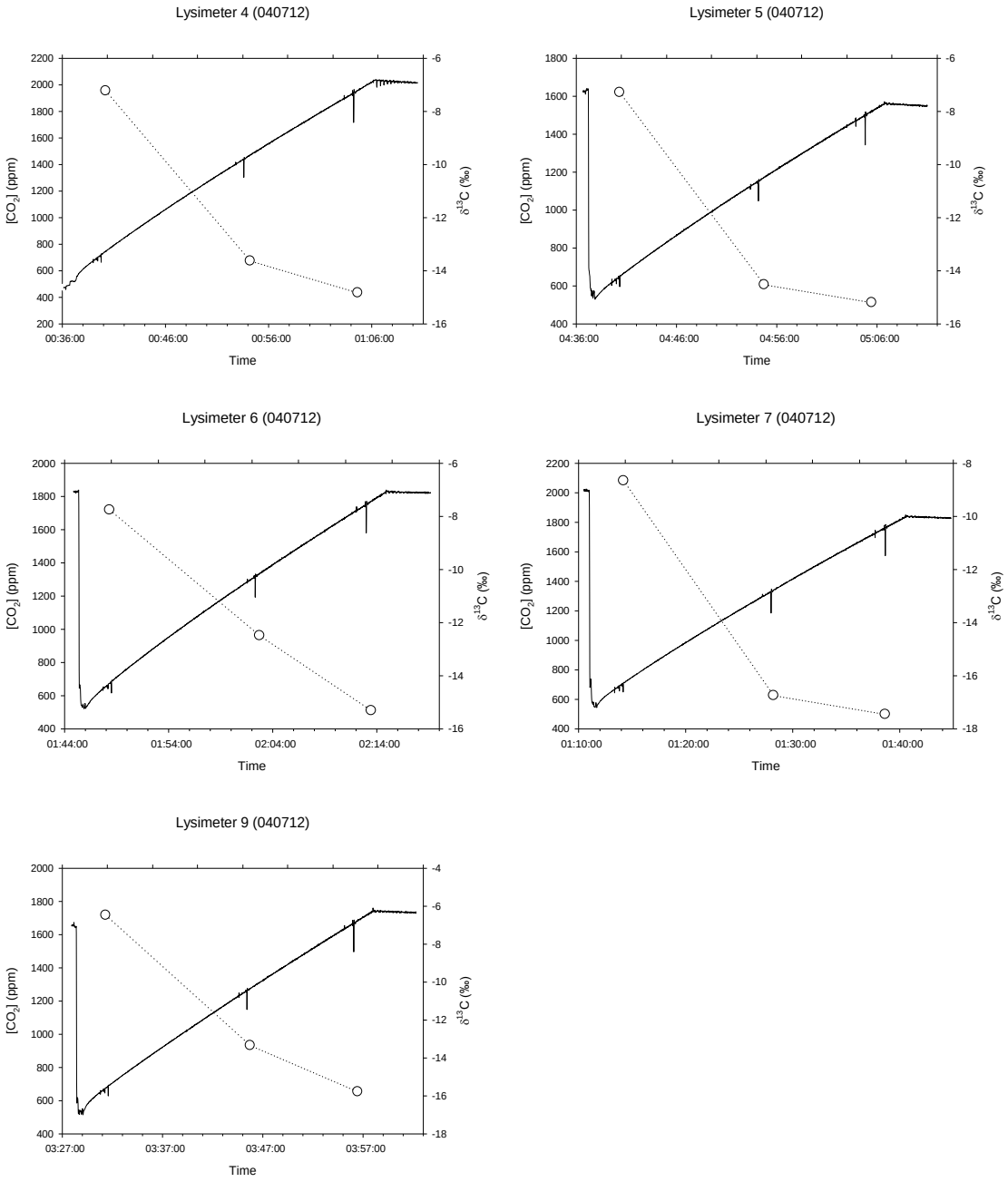

Figure 17 Plots of CO_2 concentration and isotope composition against time for night-time flux measurements in different lysimeters: (A) Shuttleworth soil and (B) Temple Balsall soil. Solid lines [CO_2]; dotted lines and circles for $\delta^{13}C$. Note the lines join adjacent points; they are not regression fits.

(A)

lys 2 040712 0253

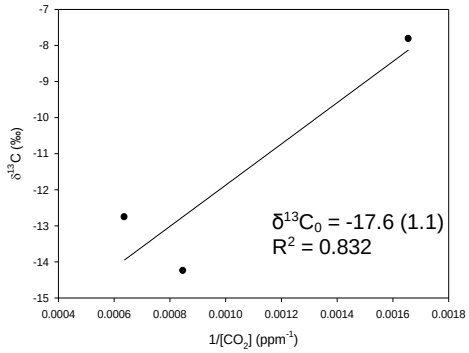

lys 2 030712 2221

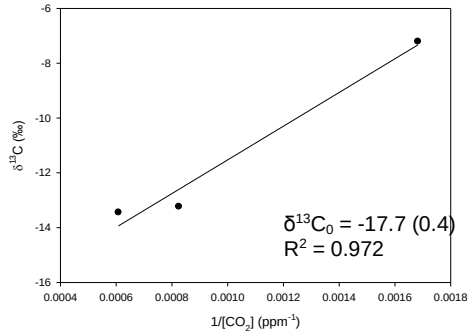

lys 2 020712 2253

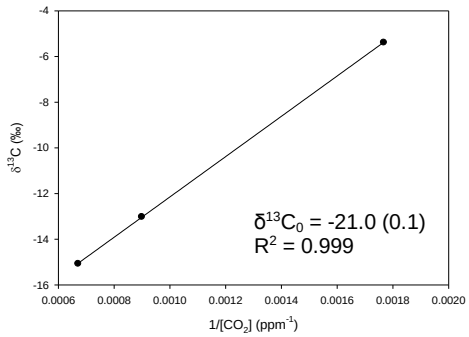

lys 3 040712 0219

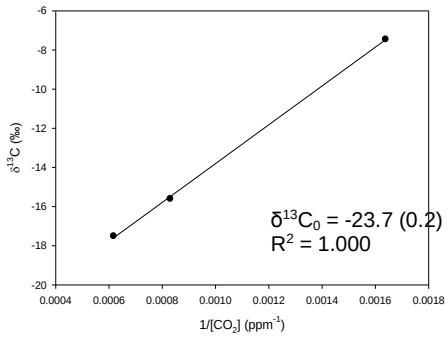

lys 3 030712 2256

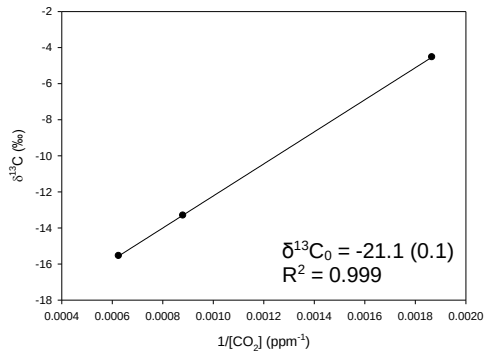

lys 8 020712 2219

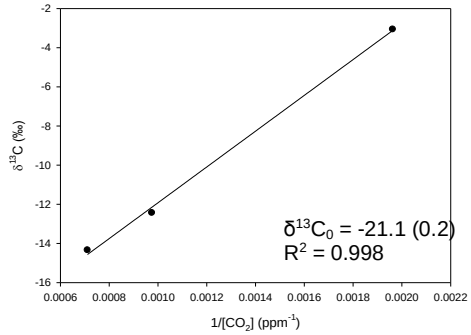

lys 10 040712 0402

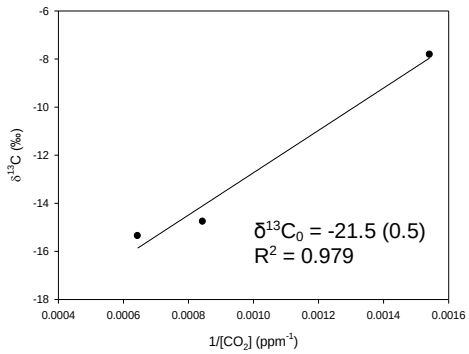

(B)

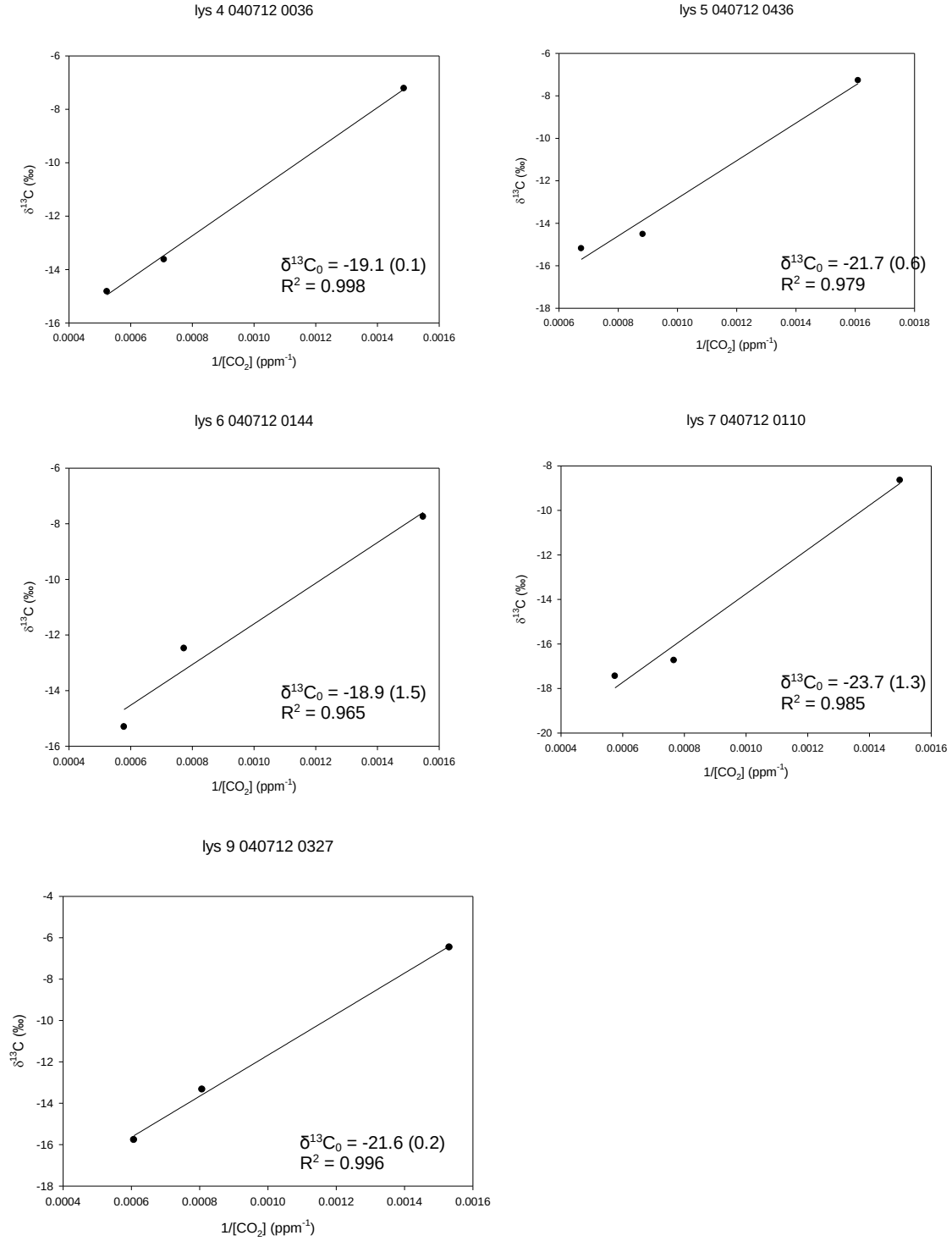

Figure 18 Keeling plots for night-time flux measurements from different lysimeters: (A) Shuttleworth soil and (B) Temple Balsall soil. $\Delta^{13}C_0$ (± 1 sd) is the intercept for the fitted regression line

The mean $\delta^{13}C$ of plant and soil respiration inferred from the mean of the individual Keeling plot intercepts is -20.5 ± 0.3 ‰ for Shuttleworth and -21.0 ± 0.7 ‰for Temple Balsall. An obvious limitation of the Keeling plots in Figure 18 is that they are made with only three isotope measurements. To extend the number of points per Keeling pots, the results from different runs were bulked for each soil, as shown in Figure 19

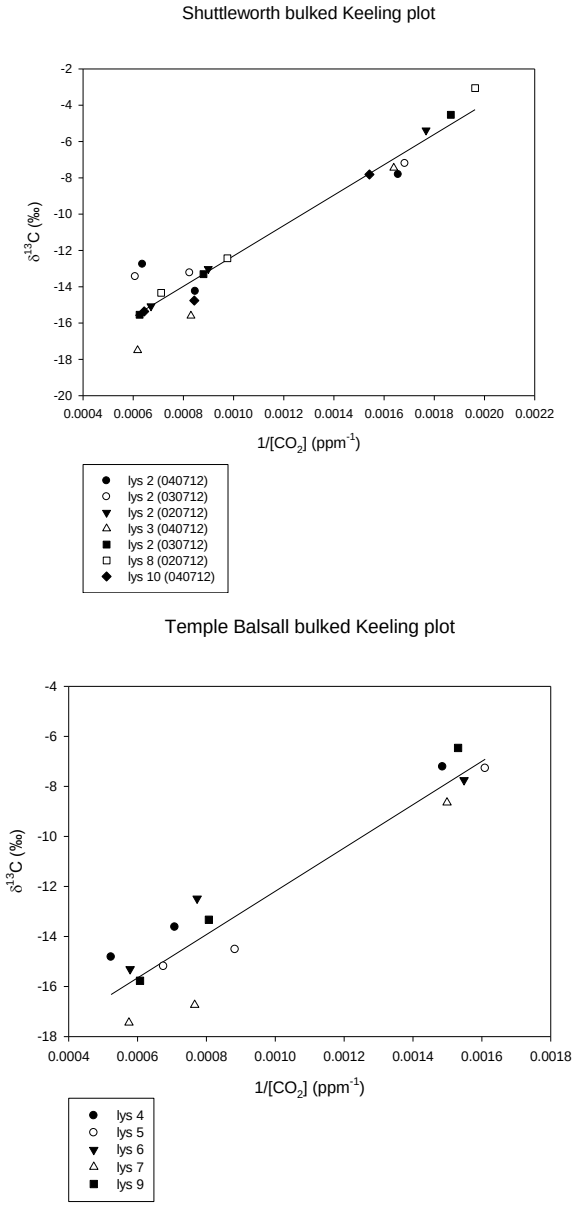

Figure 19 Keeling plots produced by grouping all soil type data together. The intercepts for these plots are; Shuttleworth = -20.67 ± 0.6 ‰ and Temple Balsall = -20.8 ± 0.8 ‰

The increased number of points allows greater confidence in the statistical significance of the fitted lines. However the fitted y-axis intercepts are not

statistically different from the mean of those of the individual Keeling plot intercepts. From Figure 19, the scatter of the data points more closely matches the regression at lower CO_2 concentrations (towards the right of the plot) compared to higher concentrations.

These measured $\delta^{13}C$ values for plant and soil respiration compare with the typical ranges for soil respiration of -22 to -24 ‰ and for plant respiration of … ‰ (refs). They are therefore on the low side of expectations.

Potential sources of error in the data and Keeling plots include:

1. Isotope measurements.
2. CO_2 concentration measurements.
3. Leaks or fractionations in the gas sampling systems.
4. Non-constant CO_2 flux into the lysimeter flux chamber.

These are discussed in turn.

Potential issues with the isotope measurements include instrumental drift and incorrect calibration. At the start of every chamber run, the IRMS is calibrated with a reference standard and drift is checked as detailed in Section 4.3.2. Hence incorrect calibration or instrument drift are unlikely to affect the isotope readings. Insufficient thawing of the cryo-prep system between samples can cause chromatogram peaks to fall outside the integrations windows, resulting in spurious isotope values. This happened if too many samples were run in the same measurement cycle in attempting to reduce analysis times. But it was not a problem for the data in Figs 5 and 6.

Potential issues with the CO_2 concentration measurements include incorrect calibration of the IRGA. The IRGA was calibrated with 0 and 300 ppm CO_2 standards on the first day of these chamber tests, and the calibration points agreed with the default the default factory settings. Subsequent servicing of the instrument by LiCor showed no drift in the calibration settings. Therefore, calibration of the IRGA is unlikely to have been an issue.

Potential issues in the gas sampling systems include gas leaks from the connections and tubing between the flux chambers and instruments, and isotope fractionations linked to leaks, gas sorption on water or other surfaces, and pressure changes. The extent of leaks was assessed in Chapter 2. It was concluded that, though small leaks were detected in some parts of the sample loops, considering the far greater volume of the whole sample loop plus chamber head space compared with the sub-sample loop tested, the leaks were unimportant. Any associated fractionation effects would also be unimportant. A potential issue in the sampling process is that the exchange of air samples for He, when samples are removed from the main sample loop for isotope analysis, may cause pressure fluctuations. This can be seen in the 'blips' in the measured CO_2 signal in Figure 17. This might introduce isotope fractionation. However, any fractionation effects would be dispersed across the whole sample loop and any effect would be minimised due to the fact that the circulating air is returned to the chamber being sampled.

This leaves potential issues associated with non-linear CO_2 flux into the lysimeter chambers. There is a possibility of bias in $\delta^{13}C$ measurements in closed chamber systems as a result of (a) the retardation effect of $^{13}CO_2$ accumulating in the chamber at a different rate to $^{12}CO_2$, due to different diffusion coefficients and concentration gradients under transient conditions; (b) a bypass effect due to differences in pressure between the chamber, soil and surrounding atmosphere, resulting in preferential flow of gas from the soil not directly beneath the chamber[46; 47]. The bypass effect does not arise in the WFL system because the soil core is isolated from its surroundings. The retardation effect is also probably small in our system. Ohlsson[46] uses solutions of the relevant diffusion equations, provided by Livingston *et al*[48], to quantify the bias in $\delta^{13}C$ arising from retardation. From his[48] Table 1; with the WFL chamber height (0.2 m), typical field soil moisture, and chamber closure times of ≤ 10 min, the bias would be approx. 0.1 ‰. However, from the plots in Figure 17, around the time the third sample was taken for isotopic analysis, the flux begins to show non-linearity. So there possibly is some fractionation due to this effect.

4.4 Conclusions

Experiments have been performed in determining sampling timescales, the accuracy and precision of isotope measurements and generation of data for Keeling plot applications.

The limitations identified have focused mainly around the timescales from measurements with the period between sampling and detection having a major influence on the number of measurements possible within a given timeframe.

Attempts at determining the accuracy and precision, although initially successful, require more work to identify the effects of individual components on the measurement process. this can include expanding the truncated sample loop to include the main sampling loop and the individual chambers.

Future experiments will also need to address the issue with the number of isotope measurements taken per flux measurement period. Increasing the number of measurements could involve the removal of the cryo loops in order to decrease the time between sampling and detection as well as avoid insufficient thawing as a result of being introduced to the liquid nitrogen too often in a short period of time. However this may cause additional errors as a result of not focusing the sample into a single pulse (as is the case where the cryo loops are used).

5 CONCLUSIONS AND FUTURE WORK

5.1 Summary of Research Performed

This research has attempted to identify the suitability and the limitations of the WFL in measuring plant and soil respiration through CO_2 concentration and $\delta^{13}C$ measurements. To this end, a series of specifications were defined such that measurements made in the WFL would be commensurate with those found elsewhere by other research groups. Experiments were then performed which identified the effects of losses within the sample loops. The methodology developed allowed for the determination of coefficients for CO_2 losses in different components of the sample loops. Additional experiments were performed with the same purpose for the $\delta^{13}C$ measurements.

Upon completion of these experiments, measurements of the flux rates in the WFL lysimeters were performed. These experiments focused of determining relative timescales for flux determination in different seasons and between the two soil types at the WFL. The results from these timescales were then instrumental in designing the experiments considering the isotopic signature of the flux. The isotope measurements of the flux were used to produce Keeling plots. Measurement cycles were performed over several days and covered entire 24 hour periods.

The limitations identified in each experiment were considered and attempts made to limit their effects in subsequent experiments. Finally, considerations were made, and are detailed below, regarding future work to be performed at the WFL.

5.2 Conclusions

5.2.1 Effects on CO_2 concentration due to loss processes (Chapter 2)

The majority of losses in the truncated sample loop were due to diffusion through the walls of plastic Bev-A line tubing. Determinations of the loss coefficients for individual components allowed for relative percentage loss compared to concentration to be identified. The percentage losses were calculated based on a 10 minute measurement period.

The main limitation arose from the use of Bev-A line tubing linking the IRGA to the sample loop. The losses were minimised by minimising the length of Bev-A line used as far as possible. Other limitations were identified from pressure pulses introduced when blowing into the truncated sample loop. This would cause additional mass-flow effects not accounted for in the CO_2 loss model developed.

5.2.2 Measurements of fluxes (Chapter 3)

Measurements of the time periods for chamber lid closure/opening, equilibration between the chamber and sample loop air were found to be independent of the environmental, temporal and spatial conditions. The measurable flux period, however was identified to be shortest in the summer when respiration rates were greatest. Comparisons between measurements showed the measurable flux period in winter was three times that in the summer. Measurements of soil temperature and moisture at depths of 60 and 120 mm, coincident with the CO_2 flux measurements, suggested greater correlation of fluxes with soil moisture than soil temperature.

The limitations identified included the need to remove the effects of photosynthesis in the chambers and to avoid non-linearity on the measured flux. The former was dealt with by blacking out the chambers – allowing for flux measurements to be performed during daylight hours. The latter involved ensuring the flux measurement period was suited to the season during which the flux measurements were being performed.

5.2.3 Measurements of flux isotopic signature (Chapter 4)

The identification of optimal sampling methods was performed and the effects of loss processes on the fractionation of the isotopic composition of the sample loop CO_2 were performed. Initial experiments towards the production of Keeling plots were performed. The results showed the isotope measurements were less reproducible than expected when setting the system specifications.

The limitations for the Keeling plots produced focused on a number of issues. Among them were sampling, measurement and flux linearity errors. The effects of these issues were explored and could account for the consistent

underestimation of the isotopic signature of plant and soil respiration compared with typical values reported in the literature. Additionally, the time period between sampling for isotopic analysis had a dominant effect on the Keeling plots produced. These issues would need to be addressed in future work.

5.3 Future Work

5.3.1 Flux measurements

Experimentation to be performed would include further consecutive 24 hour measurements of a chamber's flux, moisture and temperature to provide further information on the diurnal trends. The conclusions drawn in this research were based on the measurements of one chamber over a single 24 hour period. By extending the measurement period for a single chamber towards, for example, a 72 hour period would allow further development of the hypotheses suggested from the conclusions of this research. Using a 72 hour period as an example, two chambers per week could be analysed and could be performed throughout the year to provide additional information regarding the seasonal variation of plant and soil respiration.

5.3.2 Isotope measurements

Further experimentation is required for the effects of loss processes on the measured isotope signature of a sample to be fully understood. The initial methods used in this research should be used and should include the main sample loop and the individual chambers. The individual chamber volume would be bypassed so as to avoid any effects from plant and soil respiration. This would allow for analysis similar to that in Chapter 2 to be performed, resulting in coefficients for the individual sample loop components and provide a more detailed measure of the accuracy and precision of the WFL.

For Keeling plot applications, experiments attempting to increase the number of isotope measurements made per chamber should be performed. These experiments need to be designed such that the non-linearity in the measured flux

is avoided, whilst simultaneously ensuring full thawing on the cryo-loops. Additionally, measurements of the flux over extended periods (> 24 hours) could include isotopic analysis of the flux. This would allow diurnal and seasonal variations in the isotopic composition of plant and soil respiration to be explored.

REFERENCES

1. Read, D., Beerling, D., Cannell, M., Cox, P., Curran, P., Grace, J., Ineson, P., Jarvis, P., Malhi, Y., Powlson, D., Shepherd, J., Woodward, I., Quinn, R., Goulden, M. and Bowden, R. (2001), *The Role of Land Carbon Sinks in Mitigating Global Climate Change,* The Royal Society, London.

2. Sistani, K. R., Jn-Baptiste, M., Lovanh, N. and Cook, K. L. (2011), "Atmospheric Emissions of Nitrous Oxide, Methane, and Carbon Dioxide from Different Nitrogen Fertilizers", *Journal of environmental quality,* vol. 40, no. 6, pp. 1797-1805.

3. Berglund, O., Berglund, K. and Klemedtsson, L. (2010), "A lysimeter study on the effect of temperature on CO(2) emission from cultivated peat soils", *Geoderma,* vol. 154, no. 3-4, pp. 211-218.

4. Chapman, S. J. and Thurlow, M. (1996), "The influence of climate on CO2 and CH4 emissions from organic soils", *Agricultural and Forest Meteorology,* vol. 79, no. 4, pp. 205-217.

5. Pumpanen, J., Kolari, P., Ilvesniemi, H., Minkkinen, K., Vesala, T., Niinisto, S., Lohila, A., Larmola, T., Morero, M., Pihlatie, M., Janssens, I., Yuste, J. C., Grunzweig, J. M., Reth, S., Subke, J. A., Savage, K., Kutsch, W., Ostreng, G., Ziegler, W., Anthoni, P., Lindroth, A. and Hari, P. (2004), "Comparison of different chamber techniques for measuring soil CO2 efflux", *Agricultural and Forest Meteorology,* vol. 123, no. 3-4, pp. 159-176.

6. Minamikawa, K., Nishimura, S., Sawamoto, T., Nakajima, Y. and Yagi, K. (2010), "Annual emissions of dissolved CO(2), CH(4), and N(2)O in the subsurface drainage from three cropping systems", *Global Change Biology,* vol. 16, no. 2, pp. 796-809.

7. Lal, R., Kimble, J. M., Follett, R. F. and Stewart, B. A. (eds.) (2000), *Assessment Methods for Soil Carbon,* Lewis, Boca Raton.

8. Bellamy, P. H., Loveland, P. J., Bradley, R. I., Lark, R. M. and Kirk, G. J. D. (2005), "Carbon Losses from all Soils Across England and Wales 1978-2003", *Nature,* vol. 437, no. 8, pp. 245-248.

9. Millard, P., Midwood, A. J., Hunt, J. E., Barbour, M. M. and Whitehead, D. (2010), "Quantifying the contribution of soil organic matter turnover to forest soil respiration, using natural abundance delta C-13", *Soil Biology & Biochemistry,* vol. 42, no. 6, pp. 935-943.

10. Foley, J. A. and Ramankutty, N. (2004), "A Primer on the Terrestrial Carbon Cycle: What We Don't Know But Should", in Field, C. B. and Raupach, M. R. (eds.) *The Global Carbon Cycle: Intefrating Humans, Climate, and the Natural World,* SCOPE, .

11. Millard, P., Midwood, A. J., Hunt, J. E., Whitehead, D. and Boutton, T. W. (2008), "Partitioning soil surface CO2 efflux into autotrophic and heterotrophic components, using natural gradients in soil delta C-13 in an undisturbed savannah soil", *Soil Biology & Biochemistry,* vol. 40, no. 7, pp. 1575-1582.

12. Paterson, E., Midwood, A. J. and Millard, P. (2009), "Through the eye of the needle: a review of isotope approaches to quantify microbial processes mediating soil carbon balance", *New Phytologist,* vol. 184, no. 1, pp. 19-33.

13. Högberg, P., Nordgren, A., Högberg, M. N., Ottosson-Löfvenius, M., Bhupinderpal-Singh, Olsson, P. and Linder, S. (2005), "Fractional contributions by autotrophic and heterotrophic respiration to soil-surface CO2 efflux in Boreal forests. ", *SEB Exp Biol Ser,* , pp. 251-267.

14. Olsson, P., Linder, S., Giesler, R. and Högberg, P. (2005), "Fertilization of boreal forest reduces both autotrophic and heterotrophic soil respiration", *Global Change Biology,* vol. 11, no. 10, pp. 1745-1753.

15. Kuzyakov, Y., Friedel, J. K. and Stahr, K. (2000), "Review of mechanisms and quantification of priming effects", *Soil Biology & Biochemistry,* vol. 32, no. 11-12, pp. 1485-1498.

16. Six, J. and Jastrow, J. D. (2002), "Organic Matter Turnover", in Lal, R. (ed.) *Encyclopedia of Soil Science,* Marcel Dekker, New York, pp. 936--942.

17. Kechavarzi, C., Dawson, Q., Leeds-Harrison, P. B., SzatyLowicz, J. and Gnatowski, T. (2007), "Water-table management in lowland UK peat soils and its potential impact on CO2 emission", *Soil Use and Management,* vol. 23, no. 4, pp. 359-367.

18. Bowling, D. R., Pataki, D. E. and Randerson, J. T. (2008), "Carbon isotopes in terrestrial ecosystem pools and CO2 fluxes", *New Phytologist,* vol. 178, no. 1, pp. 24-40.

19. Boutton, T. W. (1991), "Isotope Ratios II: Environment", in Coleman, D. C. and Fry, B. (eds.) *Carbon Isotope Techniques,* Academic Press, San Diego, pp. 177.

20. Smith, K. A. and Cresser, M. S. (eds.) (2004), *Soil and Environmental Analysis: Modern Instrumental Techniques,* 3rd ed, Marcel Dekker, New York.

21. McGinn, S. M. (2006), "Measuring greenhouse gas emissions from point sources in agriculture", *Canadian Journal of Soil Science,* vol. 86, no. 3, pp. 355-371.

22. Norman, J. M., Kucharik, C. J., Gower, S. T., Baldocchi, D. D., Crill, P. M., Rayment, M., Savage, K. and Striegl, R. G. (1997), "A comparison of six methods for measuring soil-surface carbon dioxide fluxes", *Journal of Geophysical Research-Atmospheres,* vol. 102, no. D24, pp. 28771-28777.

23. Livingston, G. P., Hutchinson, G. L. and Spartalian, K. (2006), "Trace gas emission in chambers: A non-steady-state diffusion model", *Soil Science Society of America Journal,* vol. 70, no. 5, pp. 1459-1469.

24. Rayment, M. B. and Jarvis, P. G. (1997), "An improved open chamber system for measuring soil CO2 effluxes in the field", *Journal of Geophysical Research-Atmospheres,* vol. 102, no. D24, pp. 28779-28784.

25. Xu, L. K., Furtaw, M. D., Madsen, R. A., Garcia, R. L., Anderson, D. J. and McDermitt, D. K. (2006), "On maintaining pressure equilibrium between a soil CO(2) flux chamber and the ambient air", *Journal of Geophysical Research-Atmospheres,* vol. 111, no. D8, pp. D08S10.

26. Pattey, E., Edwards, G., Strachan, I. B., Desjardins, R. L., Kaharabata, S. and Riddle, C. W. (2006), "Towards standards for measuring greenhouse gas fluxes from agricultural fields using instrumented towers", *Canadian Journal of Soil Science,* vol. 86, no. 3, pp. 373-400.

27. De Klein, C. A. M., McTaggart, I. P., Smith, K. A., Stevens, R. J., Harrison, R. and Laughlin, R. J. (1999), "Measurement of nitrous oxide emissions from grassland soil using photo-acoustic infra-red spectroscopy, long-path infrared spectroscopy, gas chromatography, and continuous flow isotope-ratio mass spectrometry", *Communications in Soil Science and Plant Analysis,* vol. 30, no. 9-10, pp. 1463-1477.

28. Vance, S. (2009), "
Mars Analog Tunable Laser Spectroscopy at a Site of Active Serpentinization", *40th Lunar and Planetary Science Conference,* .

29. Wong, W. W. (1985), "Comparison of Infrared and Mass-Spectrometric Measurements of C-13 C-12 Ratios", *International Journal of Applied Radiation and Isotopes,* vol. 36, no. 12, pp. 997-999.

30. Keppler, F., Laukenmann, S., Rinne, J., Heuwinkel, H., Greule, M., Whiticar, M. and Lelieveld, J. (2010), "Measurements of (13)C/(12)C Methane from Anaerobic Digesters: Comparison of Optical Spectrometry with Continuous-Flow Isotope Ratio Mass Spectrometry", *Environmental science & technology,* vol. 44, no. 13, pp. 5067-5073.

31. Flanagan, L. B., Wever, L. A. and Carlson, P. J. (2002), "Seasonal and interannual variation in carbon dioxide exchange and carbon balance in a northern temperate grassland", *Global Change Biology,* vol. 8, no. 7, pp. 599-615.

32. Amundson, R., Stern, L., Baisden, T. and Wang, Y. (1998), "The isotopic composition of soil and soil-respired CO2", *Geoderma,* vol. 82, no. 1-3, pp. 83-114.

33. Chen, X., Post, W. M., Norby, R. J. and Classen, A. T. (2011), "Modeling soil respiration and variations in source components using a multi-factor global climate change experiment", *Climatic Change,* vol. 107, no. 3-4, pp. 459-480.

34. Midwood, A. J. and Millard, P. (2011), "Challenges in measuring the delta C-13 of the soil surface CO2 efflux", *Rapid Communications in Mass Spectrometry,* vol. 25, no. 1, pp. 232-242.

35. Maunoury-Danger, F., Boure, N. C. P., Ngao, J., Berveiller, D., Brechet, C., Dufrene, E., Epron, D., Lata, J., Longdoz, B., Lelarge-Trouverie, C., Pontailler, J., Soudani, K. and Damesin, C. (2013), "Carbon isotopic signature of CO2 emitted by plant compartments and soil in two temperate deciduous forests", *Annals of Forest Science,* vol. 70, no. 2, pp. 173-183.

36. Demeny, A. and Haszpra, L. (2002), "Stable isotope compositions of CO2 in background air and at polluted sites in Hungary", *Rapid Communications in Mass Spectrometry,* vol. 16, no. 8, pp. 797-804.

37. Nagy, Z., Pinter, K., Pavelka, M., Darenova, E. and Balogh, J. (2011), "Carbon fluxes of surfaces vs. ecosystems: advantages of measuring eddy covariance and soil respiration simultaneously in dry grassland ecosystems", *Biogeosciences,* vol. 8, no. 9, pp. 2523-2534.

38. Davidson, E. A., Savage, K., Verchot, L. V. and Navarro, R. (2002), "Minimizing artifacts and biases in chamber-based measurements of soil respiration", *Agricultural and Forest Meteorology,* vol. 113, no. 1-4, pp. 21-37.

39. Langensiepen, M., Kupisch, M., van Wijk, M. T. and Ewert, F. (2012), "Analyzing transient closed chamber effects on canopy gas exchange for optimizing flux calculation timing", *Agricultural and Forest Meteorology,* vol. 164, pp. 61-70.

40. Welles, J. M. and Mcdermitt, D. K. (2005), "Measuring carbon dioxide in the atmosphere", *Micrometeorology in agricultural systems,* , no. micrometeorolog, pp. 287-320.

41. Elsig, J. and Leuenberger, M. C. (2010), "(13)C and (18)O fractionation effects on open splits and on the ion source in continuous flow isotope ratio mass spectrometry", *Rapid Communications in Mass Spectrometry,* vol. 24, no. 10, pp. 1419-1430.

42. Crank, J. (1975), *The Mathematics of Diffusion,* 2nd ed, Oxford University Press, Oxford.

43. Liao, L. Q., Fu, Y. Z., Liang, X. Y., Mei, L. Y. and Liu, Y. Q. (2013), "Diffusion of CO2 Molecules in Polyethylene Terephthalate/Polylactide Blends Estimated by Molecular Dynamics Simulations", *BULLETIN OF THE KOREAN CHEMICAL SOCIETY,* vol. 34, no. 3, pp. 753-758.

44. Fang, C. and Moncrieff, J. (2001), "The dependence of soil CO2 efflux on temperature", *SOIL BIOLOGY & BIOCHEMISTRY,* vol. 33, no. 2, pp. 155-165.

45. Keeling, C. D. (1961), "The concentration and isotopic abubdances of carbon dioxide in rural and marine air", *Geochimica et Cosmochimica Acta,* vol. 24, pp. 277-298.

46. Ohlsson, K. E. A. (2009), "Reduction of bias in static closed chamber measurement of $\delta^{13}C$ in soil CO_2 efflux", *Rapid Communications in Mass Spectrometry,* vol. 24, pp. 180-184.

47. Nickerson N., R. D. (2009), "A numerical evaluation of chamber methodologies used in measuring the $\delta^{13}C$ of soil respiration", *Rapid Communications in Mass Spectrometry,* vol. 23, pp. 2802-2810.

48. Livingston, G. P., Hutchinson, G. L. and Spartalian, K. (2006), "Trace gas emission in chambers: A non-steady-state diffusion model", *Soil Science Society of America Journal,* vol. 70, no. 5, pp. 1459-1469.

APPENDICES

Appendix A WFL Overview

The Wolfson Field Laboratory (WFL) at Cranfield University is described. The laboratory was built for studying soil carbon dynamics and gas emissions. It contains 24 hydrologically-isolated soil monoliths (lysimeters; 12 each of two soil types) planted with grass and connected to automated gas flux chambers and instruments (Figure A1). The lysimeters are 0.8 m in diameter and 1 m deep, i.e., at least the size of a representative soil pedon, and therefore representative of field soil conditions. They are buried so that the soil surface is flush with the surroundings. Each is equipped with systems for controlling soil moisture and temperature, and instruments to allow near continuous sampling of gases emitted from the surface, dissolved solutes passing out of the bottom, and temperature and moisture at different depths.

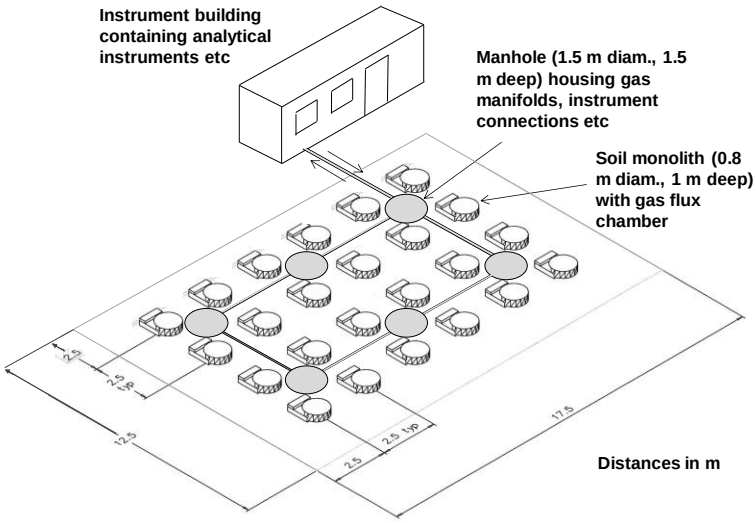

Figure A1 Plan of the site

The gas flux chambers (26-cm head space) have pneumatically operated lids. Gases accumulated when the lids are closed are passed through a continuous sampling loop to an infrared gas analyzer (IRGA) and isotope ratio mass spectrometer (IRMS) housed in an instrument building. This allows simultaneous analysis of CO_2, CH_4, N_2O, N_2 and O_2 and their C, N and O isotope compositions.

The IRMS software has been adapted to control the closing of the flux chambers and the directing of gas flow through the main sample loop to the chambers.

The lysimeters are arranged in six groups of four around six manholes to which they are connected at different depths. The manholes contain manifolds to deliver gases to the analytical instruments, collectors for the lysimeter drainage, and connections for the flux chamber pneumatics and soil heating and irrigation systems.

A.1 Technical specifications

A.1.1 Lysimeters

The soil monoliths were obtained intact (i.e. non-destructively) from field sites in the summer of 2010 and brought to Cranfield. They are contained in 5-mm thick glass fibre sleeves with galvanised iron trays at the base to collect leachate. There are two soil types: (1) a well-drained coarse loamy soil formerly under bracken/grass at Shuttleworth College, Beds, with properties (0-15 cm): pH 5.0, organic C 67 g kg^{-1}; and (2) a poorly-drained, seasonally waterlogged loamy soil over clay formerly under old pasture at Temple Balsall, Warwickshire, with properties: pH 6.0, organic C 48 g kg^{-1}. They are planted with representative pasture-grass species, now (spring 2012) in their second growing season.

The monoliths contain electrical heating elements in the surface, capable of maintaining the soil at approx. 3-cm depth at up to 5^{o}C above ambient temperature. They also have automated sprinkler irrigation systems in the flux chamber lids, delivering rainwater collected from the roof of the instrument building. Each soil monolith contains temperature and moisture sensors (Delta-T SM 300 sensors) at 5, 10, 30 and 50 cm depths, connected to data loggers. There is a complete weather station at the site, containing a Vaisala WXT520 Weather Transmitter for wind speed and direction, precipitation, atmospheric pressure, temperature and relative humidity; and Delta-T ES2 energy flux sensors for solar radiation. Data from the soil temperature and moisture sensors and weather

station are accumulated on data loggers and periodically transferred to web-accessible servers.

A.1.2 Gas flux chambers

A chamber comprises a cylindrical wall, attached to the lysimeter wall, and a pneumatically-operated lid that closes to give a gas-tight seal (Figure A2). The lid contains a 5-cm diameter vent valve which closes a few seconds after the lid to dampen pressure changes. The wall and lid are made of 10-mm thick clear acrylic plastic (Perspex). The wall is 20 cm high, so the height of the lid above the soil surface is 26 cm and the chamber volume is approx. 130 L. The chamber has been designed to be extendable if necessary. The lid opens to be well clear of the wall to avoid shading. The chamber wall is attached to the glass-fibre lysimeter wall by way of a flange and eight brackets. The brackets are designed to cope with a degree of cylindrical distortion of the lysimeter wall by the soil monolith.

Figure A2 The flux chambers

Chamber frame

The frame is welded from 304 stainless steel 50 mm box section. It is more substantial than necessary for the immediate requirements to provide scope for future modifications. Its base is carried by three brackets mounted on the lysimeter wall. The height and alignment can be adjusted. The total chamber assembly weighs 48 kg. The majority of this weight is carried on these three

mounts. The lift arm and lid are carried on two plastic bearings located in adjustable brackets on the base frame. An adjustable stop on the base frame limits the closure travel of the lift arm. The bearings are located to provide a perpendicular closure action between the lid and the chamber wall. The lid is designed to flex slightly in a diaphragm mode to provide an even seal pressure loading. The seal is a closed-cell silicone rubber foam strip, bonded to the chamber lid.

Lift arm

The lift arm is actuated by a Norgren pneumatic ram with a 63 mm diameter cylinder and end of stroke buffering. The torque requirement to raise the lid and lift arm is 82 Nm. The ram is capable of developing 1675 N of extending force, assuming 10% friction losses in the bearings and seals. The available virtual lever arm of 145 mm gives a maximum torque of 243 Nm which gives a very comfortable lift margin. The lid is held open, in an approximately vertical position, for the majority of the time. The ram load capacity is sized to resist possible wind loads on the open lid, based on UK Building Control regulations. The speed of final lid closure is varied by adjustment of the cylinder buffer bleed screw. A separate vent valve is incorporated in the lid to minimise the air pressure transient generated as the lid closes. The pneumatic circuit is arranged to ensure the vent valve automatically closes a few seconds after the lid is fully closed (next section).

Lift arm actuation

The lift actuator is operated by a two position, four-way solenoid valve connected to a compressed air supply at 5 to 7 bar. Compressed air is supplied from a Bambi 225/1000 air compressor via a particulate filter, water trap and oil lubrication system, housed in the instrument building. Restrictor orifices in the supply ports of the lift ram limit the actuation speed. When the lift is at either end of its stroke, full supply pressure builds in the appropriate side of the ram to lock it in position. The valve inlet and outlet exhausts are unrestricted. The chamber will remain fully

open unless there is a compressed air failure. In this event it will slowly close under its own weight. The end-of-stroke buffer is adjustable via a screw in the end of the cylinder. The back end of the cylinder is connected to the retraction (opening) side of the vent valve in the chamber lid. This arrangement ensures that the vent valve is fully open when the lift arm is moving, particularly during the initial opening and closure. It remains open when the lift arm is fully raised. It closes under the action of a return spring about 30 seconds after the chamber is fully lowered and remains closed until the lift arm ram is set to lift the lid. It opens a few seconds before the lid starts to rise.

A.1.3 Gas sampling system

Main sampling loop

The main sampling loop links the individual gas flux chambers to the instruments in the instrument building via manifold substations (Figure A3). The loop comprises a main ring connecting the manifold substations to the instrument building, and secondary loops connecting the manifold substations to the individual flux chambers they serve. Two further sets of loops connect the IRGA and the IRMS to the main loop in the instrument building. Air is pumped through the main loop at approx. 10 L min^{-1} at 1 atm by a Charles Austen B100 SE diaphragm pump housed in the instrument building. The pump is downstream from the IRGA and IRMS.

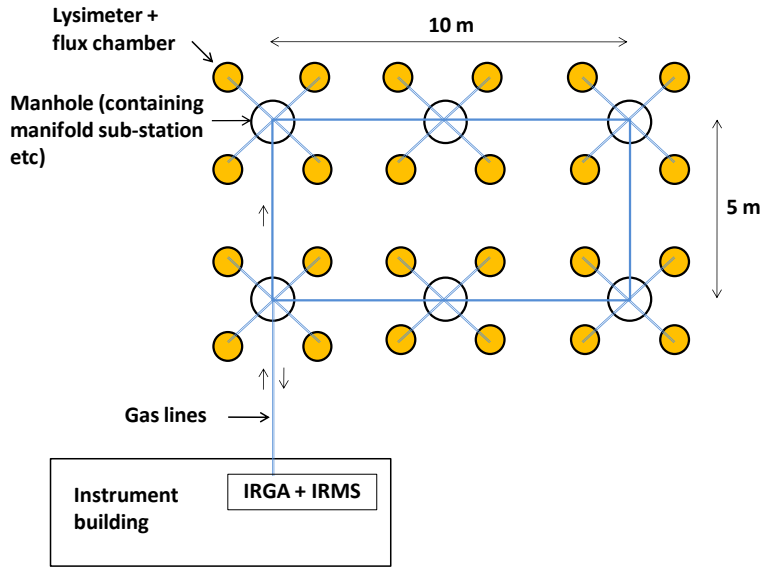

Figure A3 Schematic of the main sampling loop

The main sampling loop is made of 3/8 inch OD / 5/16 inch (7.5 mm) ID 316 stainless steel tube, polished to 0.8 μm RA and cleaned. Its total length (from a particular manifold substation to the instrument building and back) is (2 × 5) + (2 × 10) + (2 × 8) = 46 m. The manifold substations are connected to the individual gas flux chambers with ¼ inch OD / 1/8 inch (3.2 mm) ID 316 stainless steel tube. Its length for each flux chamber is (2 × 1.5) = 3 m, so the total length of the loop connecting any individual chamber to the instrument building is the same for each chamber. The total volume of air within the sampling loop (main loop plus one secondary loop to a flux chamber) is 1.9 L. This is 1.5 % of the head space in one of the flux chambers. Calculations with a pipe flow calculator and measurements with a pressure transducer show that with a flow rate of 10 L min^{-1} at 1 atm there is < 0.01 atm pressure drop across the sampling loop and associated valves.

Valve manifold system

Figure A4 shows the layout of a manifold substation. Each substation serves four lysimeter chambers, linking them to the main sampling loop in the sequence set by the IRMS software. Each substation contains eight three-port ¼ inch ID solenoid valves (SMC Pneumatics VT307-5DZ-02-Q), powered by a 24 V DC

supply, and connected by ¼ inch OD gas-impermeable nylon tubing. The control units for the valves are housed in the instrument building.

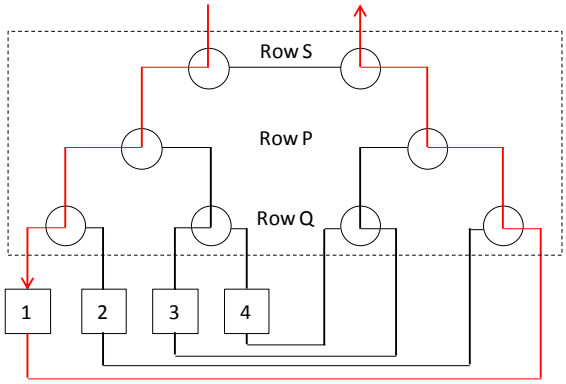

Figure A4 Valves within a manifold substation. Boxes 1-4 represent individual gas flux chambers. The valves are set for flow through chamber 1 (red lines)

The valves are arranged in three rows as shown in the figure: Rows S and P each have one pair of valves for in-flowing and out-flowing air; Row Q has two pairs. The S valves are linked to the main sampling loop and are by default set to be closed to the lysimeter chambers, i.e. the air flow bypasses the chambers. When the S valves are open, the P and Q valves direct the flow to the individual chambers. The default settings are for the S valves to flow towards the midline (i.e. bypassing the chambers) and for the P and Q valves to flow away from the midline. Hence to connect the indicated chamber the valves are changed from their default settings as follows: Row S only for Chamber 1; Rows S and Q for Chamber 2; Rows S and P for Chamber 3; and Rows S, Q and P Chamber 4.

Sampling loop for IRGA

This links the main sampling loop to the IRGA, a Licor Li840A. Air is pumped at approx. 1 L min^{-1} at 1 atm from the main stream through the IRGA using a diaphragm pump, needle valve and flow meter (Figure A5). This is the optimal rate for the IRGA; higher flow rates can damage it. The pump is a Charles Austen DA1 SE. It is located downstream from the IRGA to reduce the effects of any pressure fluctuations it causes, which could introduce noise in the IRGA readings. The piping for the subsample loop is 1/4 inch OD / 1/8 inch ID PTFE tube.

Measurements with a pressure transducer show that this arrangement produces pressure fluctuations < 0.01 atm at the IRGA. This is well within the IRGA's tolerance.

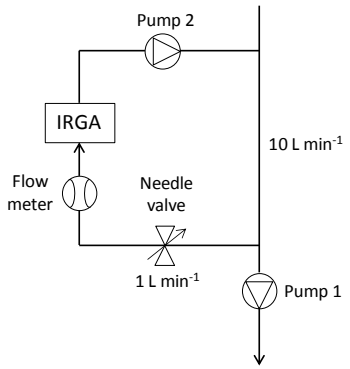

Figure A5 The sampling loop for the IRGA

Sampling loop for IRMS

This links the main sample loop to the sample prep unit of the IRMS, a SerCon 20-22 with a CryoPrep unit (Sercon 2010). Figure A6 shows the loop's components and Figure A7 shows its relation to the main loop and sample prep unit. The loop comprises three two-position six-port Valco valves with 3/8 inch-equivalent internal plumbing, connected to three sub-loops of increasing volume for gases of decreasing abundance: 5 mL for N_2 and O_2; 10 mL for CO_2; and 250 mL for CH_4 and N_2O. The individual loops are made of the same 3/8 inch stainless steel tubing as the main sampling loop. Their lengths are 5 cm, 25 cm and 5 m for N_2/O_2, CO_2 and CH_4/N_2O, respectively. During a sampling event (i.e. closure of a particular flux chamber's lid), the air in the whole loop is allowed to equilibrate with the air in the chamber (taking a few minutes), then the contents of the three sample loops are injected into the prep unit, as shown in Figure A6.

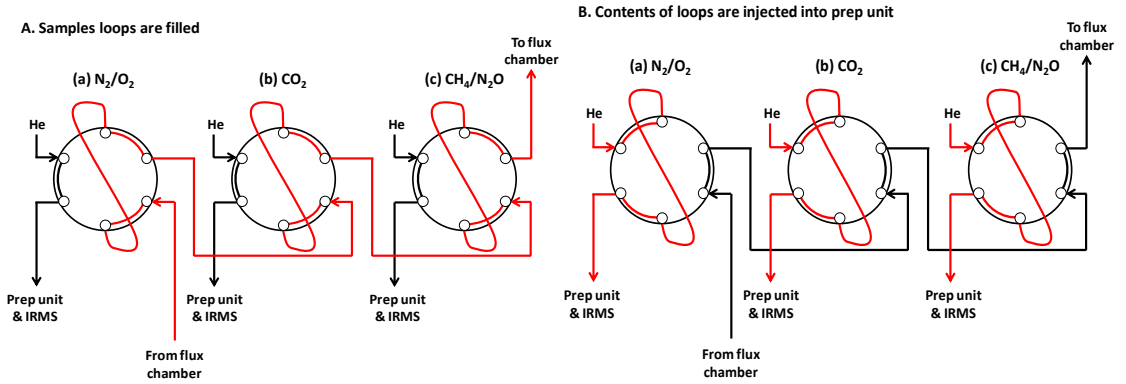

Figure A6 The IRMS sample loops. The red lines show the flow through the Valco valves and sample loops. In Position A, the sample loops are filled; in Position B, the contents of the loops are injected into the prep unit and IRMS

Sample prep unit for IRMS

Figure A7 shows the prep unit. It shows three paired gas lines from top to bottom. The topmost line in each pair is for the He carrier gas; the lower line is for the sampled gas. From bottom to top the sampled gases are:

a. N_2 and O_2, passing through a water trap (Nafion), a 5A molecular sieve gas chromatography column (GC3), and then to the IRMS.
b. CO_2, passing through a water trap, cryo-focus unit, a Poropack QS column (GC2) and then to the IRMS.
c. CH_4 and N_2O, passing through a water trap, CO oxidizer (Schütze reagent), CO_2 scrubber (Carbosorb), cryo-trap unit for N_2O, furnace for oxidizing CH_4 to CO_2, cryo-trap unit for CO_2 generated from CH_4, cryo-focus unit, a Poraplot column (GC1), and then to the IRMS.

After N_2O is frozen on the first cryo-trap loop, CH_4 is passed through to be combusted to CO_2, then cryo-trapped and cryo-focused on the two remaining cryo-loops. The CO_2 then passes onto GC1 and so to the IRMS. When the third cryo-loop (cryo-focus) is thawing, the N_2O is released from the first cryo-trap 1, and refrozen on the second cryo-trap. Finally it is cryo-focused and passed on to GC1 and the IRMS.

The CH_4/N_2O line in Figure A7 is also connected to an auto-sampler unit (*via* Valves 1 and 2). Samples from the auto-sampler can be analyzed for CO_2 (the

CO_2 scrubber is bypassed), CH_4, N_2O, N_2 and O_2. Reference gases are introduced at the IRMS inlet. A total of 15 valves control the flow through the sample preparation unit.

A.2 Control of the Sampling Process

The sampling system is controlled by the Callisto CF_IRMS software for stable isotope ratio analysis on SerCon mass spectrometers and prep systems (SerCon 2009). Callisto is used to control the available functions of the mass spectrometer and prep system, to collect data and to process it to give the isotopic enrichments of samples. In the WFL, it is also used to control the opening and closing of the chamber lids and the switching of all valves in the sample loops. Table A1 lists the components under Callisto control.

In Callisto terminology, the valve controls are located on ‘nodes’. In total, there are four such nodes: two for the gas sampling system, one for the sample prep system and one for the IRMS. Each node contains two ‘cards’ containing 16 valve controls, which are used for individual valves, groups of valves (as with the manifold valve system) and the chamber lid actuators.

Table A1 Components controlled by the Callisto software. See text for explanation

Component	Number of valve controls	Identifiers in Callisto Sequence Table		
		Nodes	Cards	Valve controls
Main sampling loop valves	18	1 & 2	Both on Node 1, first on Node 2	0–2 & 8–10 on each card
Chamber lid actuator switches	24	1 & 2	As above	3–6 & 11–14 on each card
IRMS sample loop valves	3	U	2	5–7
Prep unit valves	15	U	1 & 2	0–12 on Card 1, 1–2 on Card 2
Prep unit cryo-loop switches	4	U	1 & 2	13–15 on Card 1, 0 on Card 2
Reference gas valves	3	#	2	0–2
IRMS switches	2	#	2	5–6

Callisto is based on the Microsoft Windows operating system. Control and sequencing of switches and valves is made through Setup Groups, accessed via an icon in the Master Window toolbar. A Setup Group defines the experimental timings, gas species, integration windows, outputs, references and sequences for a particular analysis. It includes a Sequence Table, which determines the valves/switches to be operated and when. The Table has three columns: Time to specify when an Event occurs; Events to specify the operations performed; and L/R to specify whether the Event is associated with the prep system (Local) or with the mass spec (Remote). The WFL gas sampling system is treated as Local (i.e. part of the prep system). Valve or switch node addresses are specified in the Sequence Table according to the syntax:

Node; Control; Card; ON/OFF

where Node is 1, 2, U or # for the four nodes; Control is 0–15 for the 16 valve controls on a given card; Card is either VALVE or VALV2 for Cards 1 and 2 on a given node; and ON/OFF refers to the power supply to the valve or switch. Valves can be normally open, normally closed or three way; switching ON or OFF will have the corresponding effect.

The example in Table A2 gives the Events to connect Chamber 3 (cf Figure A7) to the main sampling loop and close the chamber lid (see A.1.3 for the arrangement of valves in Rows S, P and Q).

Table A2 Events in a Callisto Sequence Table to connect Chamber 3 to the sampling loop and close its lid

Event	Consequence
1 0 VALVE OFF	Row Q valves at default
1 1 VALVE ON	Row P valves activated
1 2 VALVE ON	Row S valves activated
1 5 VALVE ON	Chamber 3 lid closed

During a set of measurements of gas fluxes from the 24 lysimeters, the software needs to close and open the chamber lids in a random sequence, and to open the relevant valves in the gas sampling loops. During the interval between one lid closing and the next closing, there are four sub-intervals:

i. the time required for the lid to close, Δt_1 (approx. 0.5 min);
ii. the time required for the air in the closed chamber and gas lines to equilibrate, Δt_2 (approx. 2 min);
iii. the time required for the flux measurement, Δt_3 (at least 5 min, depending on the gas or gases being analysed); and
iv. the time required for the gas lines to re-equilibrate with the external atmosphere after the lid opens, Δt_4 (approx. 2 min).

The time between the start of the lid closing and the start of the lid opening ($\Delta t_1 + \Delta t_2 + \Delta t_3$) and the time from then to the start of the next lid closing (Δt_4) are

specified in the relevant Sequence Table in Callisto. The software randomises the sequence of closings in each cycle of measurements.

The software also sends a signal to the IRGA software letting it know which lid closed when, and it triggers irrigation events in the lysimeters, as well as controlling the IRMS prep and analysis operations.

A.3 References

SerCon (2009) Callisto CF_IRMS. *Stable isotope ratio analysis, data collection and processing software*. Version 2.1. SerCon Ltd, Crewe, Cheshire.

SerCon (2010) *Cryo prep trace gas analyser user's manual*. Version 1.0. SerCon Ltd, Crewe, Cheshire.

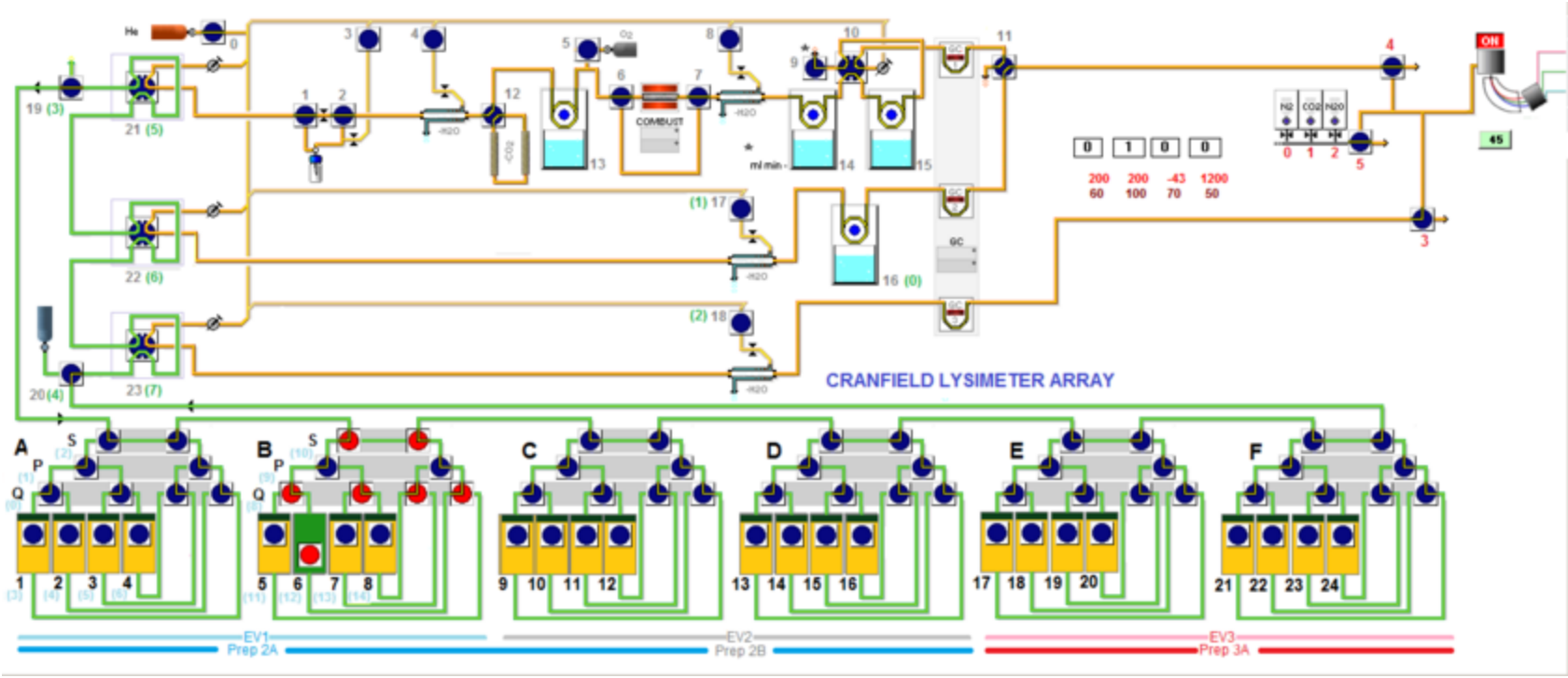

Figure A7 Schematic of the main sampling loop and valve manifold system (green lines), and the secondary sampling loops and preparation units for the IRMS (orange lines). Valves coloured red are open for sampling; valves coloured blue are closed. See text for explanation